Journal of Computational Physics 228 (2009) 7771–7791

Contents lists available at ScienceDirect

Journal of Computational Physics

journal homepage: www.elsevier.com/locate/jcp

Higher-order quadrature-based moment methods for kinetic equations

R.O. Fox *

Department of Chemical and Biological Engineering, 2114 Sweeney Hall, Iowa State University, Ames, IA 50011-2230, USA

ARTICLE INFO

Article history:
Received 15 December 2008
Received in revised form 15 July 2009
Accepted 21 July 2009
Available online 26 July 2009

Keywords:
Quadrature method of moments
Velocity distribution function
Kinetic equation
Rarefied gas flows
Boltzmann equation
Dilute particle flows

ABSTRACT

Kinetic equations containing terms for spatial transport, body forces, and particle–particle collisions occur in many applications (e.g., rarefied gases, dilute granular gases, fluid-particle flows). The direct numerical solution of the kinetic equation is usually intractable due to the large number of independent variables. A useful alternative is to reformulate the problem in terms of the moments of the velocity distribution function. Closure of the moment equations is challenging for flows sufficiently far away from the Maxwellian limit. In previous work, a quadrature-based third-order moment closure was derived for approximating solutions to the kinetic equation for arbitrary Knudsen number. A key component of quadrature-based closures is the moment-inversion algorithm used to find the non-negative weights and velocity abscissas. Here, a robust inversion procedure is proposed for three-component velocity moments up to ninth order. By reconstructing the velocity distribution function, the spatial fluxes in the moment equations are treated using a kinetic-based finite-volume solver. Because the quadrature-based moment method employs the moment transport equations directly instead of a discretized form of the kinetic equation, the mass, momentum and energy are conserved for arbitrary Knudsen and Mach numbers. The computational algorithm is tested for the Riemann shock problem and, for increasing Knudsen numbers (i.e. larger deviations from the Maxwellian limit), the accuracy of the moment closure is shown to be determined by the discrete representation of the spatial fluxes.

1. Introduction

The kinetic equation for the velocity distribution function is used in many applications [2,8–10,12,26,28,30,32–34,50,54,62], and thus there have been many computational methods developed to find approximate solutions. At present, there are two classes of methods that can be used to find accurate solutions to the kinetic equation: (i) direct solvers that discretize velocity phase space [2,7,27,49,50] and (ii) Lagrangian methods [4]. However, the computational cost of using either of these methods in many applications is prohibitive. Moreover, in most applications we are not interested in knowing the exact form of the velocity distribution function, rather knowledge of its lower-order moments is sufficient [57]. For these reasons, there is considerable motivation to develop predictive moment closures whose accuracy can be improved in a rational manner [30,41,58]. Quadrature-based moment closures [16,19,21,42] fall into this category because, in principle, the accuracy of these closures can be improved by increasing the number of quadrature nodes [29,45]. Nevertheless, a key technical challenge with quadrature-based moment closures is the development of efficient moment-inversion algorithms for three-dimensional velocity moments [21] that can be extended to reconstruct the velocity distribution function using higher-order moments.

We should note that because the weights are non-negative and the velocity abscissas are located in velocity phase space, a quadrature-based moment method provides a *realizable* discretization of velocity phase space that is consistent with the underlying moments [17]. Moreover, if integer moments up to order γ are used in the moment-inversion algorithm, the

* Tel.: +515 294 9104; fax: +515 294 2684.
E-mail address: rofox@iastate.edu

0021-9991/$ - see front matter © 2009 Elsevier Inc. All rights reserved.
doi:10.1016/j.jcp.2009.07.018

quadrature-based estimation of the moment of order $\gamma + 1$ is optimal in the sense that it is closest to the true value and has the smallest possible error [29,61]. Compared to direct solvers, the quadrature-based discretization of velocity phase space is very sparse (equal to the number of quadrature nodes). An important open question is thus to determine the range of accuracy that can be achieved using quadrature in comparison to direct solvers. Generally, in order to improve the accuracy for finite Knudsen numbers, the number of quadrature nodes (and hence the number of transported velocity moments) must be increased. In [21] the moment-inversion algorithm was limited to 8-node quadrature and 14 velocity moments up to third order. In this work, we address the problem of finding a moment-inversion algorithm for higher-order velocity moments. In particular, we describe an algorithm for computing an n^3-node quadrature using $(n^2 + 3)n$ velocity moments, where n is the number of quadrature nodes in each direction. In order to verify the higher-order moment-inversion algorithm, we combine it with a kinetic-based finite-volume method to solve the Riemann shock problem with 8-, 27- and 64-node quadratures using 14, 36 and 76 moments, respectively, at finite Knudsen numbers.

As discussed in detail elsewhere [21], quadrature-based moment methods are related to other discrete velocity models for the Boltzmann equation [7,25,27,36,49], but perhaps most closely related to off-lattice Boltzmann methods (oLBM) [1]. The principal difference with oLBM is that in a quadrature-based moment method the velocity abscissas are computed (along with the weights) directly from the moments instead of being held fixed. As in other quadrature methods [19,20,29,43–45,61,66], allowing the weights and abscissas to adapt to the underlying moments of the distribution function greatly increases the order of accuracy that can be obtained with a given number of abscissas. However, because moment inversion with variable abscissas is highly nonlinear [55] and notoriously ill-conditioned [52], computation of the abscissas must be done with the appropriate algorithms [29,52,61]. As shown in [21], allowing the velocity abscissas to vary at every point in the flow has many advantages. For example, the treatment of high Mach number flows is not an issue, as well as flows with arbitrary Knudsen numbers. Moreover, in the low-Mach-number limit, the velocity abscissas in the quadrature-based moment method described in this work approach the same values as those used in oLBM [1] (i.e., they correspond to the zeros of the Hermite polynomial of order n). In general, for quadrature-based moment methods the abscissas will be the zeros of an orthogonal polynomial whose weighting function is the (unknown) velocity distribution function [17,55], and the computational algorithms used to compute the abscissas exploit this relationship [29,52,61].

Quadrature-based moment methods also share some common features with gas-kinetic schemes [14,31,64,65]. In particular, both methods use velocity moments to reconstruct the velocity distribution function in order to compute the spatial fluxes at the cell interfaces. Thus, the principle difference between the two methods is how the distribution function is reconstructed from the moments. For gas-kinetic schemes, the distribution function is assumed to be close to a Maxwellian distribution; hence, the method is ideally suited for gas flows with small Knudsen number (i.e., highly collisional gas flows). In quadrature-based moment methods [29,61], the reconstructed distribution function is a finite set of weighted Dirac delta functions that exactly reproduces the set of transported velocity moments. This reconstruction method offers several advantages for treating kinetic equations with arbitrary Knudsen number (e.g. collision-less gases) and kinetic equations for physical problems with additional physics (e.g., fluid-particle and fluid-droplet flows with finite Stokes number and/or droplet coalescence [15,16,21,23,34,37,38,54,62]). Nevertheless, the methodology [47,48,64] used to increase the spatial/temporal accuracy in gas-kinetic schemes should be directly applicable to quadrature-based moment methods. Finally, we should note that for gas flows near the Maxwellian limit (e.g. low Knudsen number) and for low-Mach number (i.e. incompressible) flows, the efficient distribution reconstruction algorithm used in gas-kinetic schemes should be much faster than quadrature-based reconstruction. However, for general kinetic equations far from equilibrium, the quadrature-based reconstruction offers many advantages [21], such as the ability to describe crossing jets of particles in the collision-less limit [13,15,16,24].

The remainder of the paper is organized as follows. In Section 2 we introduce the kinetic theory for dilute particle flows, where we use the term "particle" in the generic sense (i.e., hard spheres, molecules, droplets, etc.). Section 3 describes in detail the quadrature-based moment-inversion method for the three-component velocity moments up to ninth order. In Section 4 we review the kinetic-based numerical algorithm used to solve the velocity moment transport equations. Section 5 is devoted to an example application (Riemann shock problem) to test the numerical implementation and, in particular, to evaluate how the numerical solutions depend on the number of quadrature nodes used in the reconstruction for a given value of the Knudsen number. Finally, in Section 6 conclusions are drawn and the key characteristics of the proposed quadrature-based moment method and numerical algorithm are discussed.

2. Kinetic theory of dilute particle flows

2.1. Kinetic equation

Consider the following kinetic equation for the velocity distribution function $f(\mathbf{v};\mathbf{x},t)$ of dilute monodisperse particles:

$$\partial_t f + \mathbf{v}\cdot\partial_{\mathbf{x}} f + \partial_{\mathbf{v}}\cdot(\mathbf{g}f) = \mathbb{C}, \tag{1}$$

where $\mathbf{v} = (v_1, v_2, v_3)$ is the particle velocity vector, $\mathbf{g} = (g_1, g_2, g_3)$ is a body force,[1] and $\mathbb{C}$ is the particle–particle collision term. In this work, we will assume that the collision term can be closed using the Bhatnagar–Gross–Krook (BGK) approximation [3]:

[1] For fluid-particle flows, a velocity-dependent force, which is inversely proportional to the Stokes number, is required. The treatment of such terms is described in [21]. Here, we consider a system with infinite Stokes number.

$$\mathbb{C} = \frac{1}{\tau}(f_{\text{eq}} - f) \tag{2}$$

where τ is a collision time constant and f_{eq} is the Maxwellian distribution. In three dimensions,[2] f_{eq} is given by

$$f_{\text{eq}}(\mathbf{v}) = \frac{\rho}{(2\pi\sigma_{\text{eq}})^{3/2}} \exp\left(-\frac{|\mathbf{v}-\mathbf{U}|^2}{2\sigma_{\text{eq}}}\right) \tag{3}$$

where $\rho = \int f \, d\mathbf{v}$ is the particle number density (zero-order moment), and $\mathbf{U}$ and σ_{eq} are the mean particle velocity and equilibrium variance, respectively. For elastic collisions, σ_{eq} is a conserved quantity. Note that the Knudsen number is proportional to the collision time τ, so that the velocity distribution function is equal to f_{eq} when $Kn = 0$. In the opposite limit, the particles are collision-less and the velocity distribution function will be determined by the terms on the left-hand side of Eq. (1). As we shall see below, the advantage of using the BGK approximation is that the moment equations derived from the collision term are closed [57]. However, this is not a requirement and the quadrature-based moment method could also be used to close the collision term [59]. In this work, our main interest is the closure of the transport term $(\mathbf{v}\cdot\partial_{\mathbf{x}} f)$ using moment methods for spatially inhomogeneous flows (e.g. the Riemann shock problem), so the BGK approximation will be adequate.

2.2. Moment transport equations

Our principal interest is to develop moment closures using quadrature-based moment methods that employ moments of increasing order. Let M^{γ}_{ijk} denote the velocity moment of order $\gamma = i+j+k$, where the non-negative integers i,j,k denote the orders for each velocity component:[3]

$$M^{\gamma}_{ijk}(\mathbf{x},t) \equiv \int v_1^i v_2^j v_3^k f(\mathbf{v};\mathbf{x},t)\, d\mathbf{v}. \tag{4}$$

Likewise, let

$$\Delta^{\gamma}_{ijk}(\mathbf{x},t) \equiv \int v_1^i v_2^j v_3^k f_{\text{eq}}(\mathbf{v};\mathbf{x},t)\, d\mathbf{v} \tag{5}$$

denote the moments of the equilibrium distribution. The transport equations for the moments can be found starting from Eq. (1) [57]:

$$\partial_t M^{\gamma}_{ijk} + \partial_{x_1} M^{\gamma+1}_{i+1jk} + \partial_{x_2} M^{\gamma+1}_{ij+1k} + \partial_{x_3} M^{\gamma+1}_{ijk+1} = ig_1 M^{\gamma-1}_{i-1jk} + jg_2 M^{\gamma-1}_{ij-1k} + kg_3 M^{\gamma-1}_{ikj-1} + \frac{1}{\tau}\left(\Delta^{\gamma}_{ijk} - M^{\gamma}_{ijk}\right). \tag{6}$$

By convention, the moments with negative subscripts resulting from the body-force term are null. Note that for a given order γ this equation is not closed due to the spatial flux terms of order $\gamma+1$ involving $M^{\gamma+1}_{i+1jk}, M^{\gamma+1}_{ij+1k}$ and $M^{\gamma+1}_{ijk+1}$. On the other hand, the terms due to body forces and collisions are closed.

As noted above, the particle density corresponds to the moment of order zero. The three components of the mean velocity vector $\mathbf{U}$ are defined in terms of the first-order moments:

$$M^1_{100} \equiv \rho U_1, \quad M^1_{010} \equiv \rho U_2, \quad M^1_{001} \equiv \rho U_3. \tag{7}$$

The second-order moments are used to define the velocity covariance matrix [21], denoted here by $\sigma_U = [\sigma_{\alpha\beta}]$. The trace of σ_U is proportional to the particle temperature, and we define $\sigma_{\text{eq}} \equiv (\sigma_{11}+\sigma_{22}+\sigma_{33})/3$. Conservation of mass, momentum and energy during collisions yield, respectively,

$$\begin{aligned}
&\Delta^0_{ijk} = \rho,\\
&\Delta^1_{100} = \rho U_1, \quad \Delta^1_{010} = \rho U_2, \quad \Delta^1_{001} = \rho U_3,\\
&\Delta^2_{ijk} = \rho\left(\sigma_{\text{eq}} + U_1^2\right)\delta_{i2} + \rho\left(\sigma_{\text{eq}} + U_2^2\right)\delta_{j2} + \rho\left(\sigma_{\text{eq}} + U_3^2\right)\delta_{k2} + \rho(U_1U_2\delta_{ij} + U_1U_3\delta_{ik} + U_2U_3\delta_{jk}),
\end{aligned} \tag{8}$$

where δ_{ij} is the Kronecker delta. For higher-order moments, Δ^{γ}_{ijk} depends uniquely on $\rho, \mathbf{U}$ and σ_U.

In quadrature-based moment methods [15,16,21], the spatial fluxes appearing in Eq. (6) are represented by a kinetic description [6,14,51,53]. First, the components of the flux vector for moment M^{γ}_{ijk} are decomposed into two contributions:

$$\begin{aligned}
M^{\gamma+1}_{i+1jk} &= Q^-_{1,ijk} + Q^+_{1,ijk},\\
M^{\gamma+1}_{ij+1k} &= Q^-_{2,ijk} + Q^+_{2,ijk},\\
M^{\gamma+1}_{ijk+1} &= Q^-_{3,ijk} + Q^+_{3,ijk},
\end{aligned} \tag{9}$$

[2] For clarity, we will only consider 3-D flows in this work. However, it is straightforward to reduce the moment equations and quadrature formulas to treat 1-D and 2-D flows.

[3] Note that this definition uses different subscripts to denote the moments than was used in [21] and elsewhere [57]. The new notation was adopted to facilitate the ordering of moments of high order.

where the nth component of each contribution is defined in terms of the velocity distribution function:

$$Q^-_{n,ijk} \equiv \int \min(v_n, 0)\, v_1^i\, v_2^j\, v_3^k f(\mathbf{v})\, \mathrm{d}\mathbf{v},$$
$$Q^+_{n,ijk} \equiv \int \max(v_n, 0)\, v_1^i\, v_2^j\, v_3^k f(\mathbf{v})\, \mathrm{d}\mathbf{v}. \tag{10}$$

In quadrature-based moment methods f is reconstructed as a point distribution function using the moments (i.e. as a sum of Dirac delta functions with non-negative weights). Thus, $Q^-_{n,ijk}$ and $Q^+_{n,ijk}$ will be known at every point in the flow, and can be used (e.g., with a finite-volume discretization [40]) to compute the spatial flux terms in the moment transport equation (Eq. (6)). We will discuss the computation on the spatial fluxes in more detail in Section 4. However, based on the analysis of [29], we should expect that using quadrature to estimate $M^{\gamma+1}_{ijk}$ from the moments $M^n_{ijk}, n \in (0, 1, \ldots, \gamma)$ will be close to optimal.

2.3. Rotated central moments

The moment-inversion algorithm used in quadrature-based moment methods is constructed using a linear transformation of the central moments [21]. The latter are defined by

$$C^\gamma_{ijk}(\mathbf{x}, t) \equiv \int (v_1 - U_1)^i (v_2 - U_2)^j (v_3 - U_3)^k f(\mathbf{v}; \mathbf{x}, t)\, \mathrm{d}\mathbf{v}. \tag{11}$$

The central moment C^γ_{ijk} can be expressed uniquely in terms of the set of all moments up to order γ : $\left(M^0_{ijk}, M^1_{ijk}, \ldots, M^\gamma_{ijk}\right)$ [21,57]. It is thus possible to write transport equations for each of the central moments starting from Eq. (6) [57]. In principle, either system of moment equations can be used with quadrature-based moment methods as long as the spatial fluxes are treated in an equivalent manner (i.e. using Eq. (9)). For the purposes of constructing a realizable quadrature, the optimal set of moments to transport is not the central moments, but rather the rotated central moments defined by

$$R^\gamma_{ijk}(\mathbf{x}, t) \equiv \int \left[\sum_{\beta=1}^{3} L_{1\beta}(v_\beta - U_\beta)\right]^i \left[\sum_{\beta=1}^{3} L_{2\beta}(v_\beta - U_\beta)\right]^j \left[\sum_{\beta=1}^{3} L_{3\beta}(v_\beta - U_\beta)\right]^k f(\mathbf{v}; \mathbf{x}, t)\, \mathrm{d}\mathbf{v}, \tag{12}$$

where the unitary matrix $\mathbf{L}(\mathbf{x}, t) = [L_{\alpha\beta}]$ depends on the local velocity covariance σ_U. More specifically, let $\mathbf{c} = \mathbf{v} - \mathbf{U}$ denote the fluctuating (or particular) velocity vector, and let $\mathbf{r} = \mathbf{L}\mathbf{c}$. By construction, $\mathbf{L}$ is defined such that the covariance matrix for $\mathbf{r}$, denoted by σ_R, is diagonal [21]. Thus, $R^2_{110} = R^2_{101} = R^2_{011} = 0$.[4] For example, if σ_U is diagonal (e.g., as in the Riemann shock problem), then $\mathbf{L} = \mathbf{I}$ so that $\sigma_R = \sigma_U$ and $R^\gamma_{ijk} = C^\gamma_{ijk}$.

In general, the rotated central moment R^γ_{ijk} can be expressed uniquely in terms of the set of all moments up to order γ : $\left(M^0_{ijk}, M^1_{ijk}, \ldots, M^\gamma_{ijk}\right)$ [21]. Thus, an optimal implementation of quadrature-based moment methods would solve the transport equation for the rotated central moments. Hereinafter we will assume that the rotated central moments are known (or can be computed from the set of transported moments) and focus on the moment-inversion algorithm needed to find the quadrature weights and velocity abscissas from R^γ_{ijk}. As described in [21] (and discussed in detail below), the velocity abscissas consist of a finite set of N velocity vector fields $\mathbf{U}_\alpha(\mathbf{x}, t)$ where $\alpha \in (1, \ldots, N)$. The moment-inversion algorithm for R^γ_{ijk} will provide a set of N rotated and translated velocity vector fields $\mathbf{R}_\alpha(\mathbf{x}, t)$. The key relation between the two sets of velocity fields is

$$\mathbf{R}_\alpha = \mathbf{L}(\mathbf{U}_\alpha - \mathbf{U}) \Longleftrightarrow \mathbf{U}_\alpha = \mathbf{L}^{\mathrm{T}}\mathbf{R}_\alpha + \mathbf{U} \tag{13}$$

where $\mathbf{L}$ and $\mathbf{U}$ are known from the lower-order moments ($\gamma \leqslant 2$). The weights ρ_α remain the same in either representation [21]. In the next section we present a method for computing ρ_α and $\mathbf{R}_\alpha$ given R^γ_{ijk} for $N = n^3$ with $n \in (1, 2, 3, \ldots)$.

In summary, the set of discrete velocity abscissas used in quadrature-based moment methods (Eq. (13)) are translated with respect to the mean velocity $\mathbf{U}$ and rotated using $\mathbf{L}$ into a stress-free (diagonal) coordinate system. The translation ensures that the quadrature remains Galilean invariant and realizable (i.e. non-negative weights) for arbitrary Mach number. The rotation is required to ensure that the quadrature remains realizable when the velocity covariances are far from zero. (Negative weights can be found for non-rotated systems even when the normalized velocity distribution function is Gaussian.) As discussed elsewhere [21], quadrature-based moment methods offer several advantages over discrete velocity methods with fixed abscissas [1,7,25,27,35,36,49], perhaps the most significant of which is the ability to treat non-isothermal flows at arbitrary Mach number. (With fixed abscissas, the weights will eventually become negative as the Mach number increases from zero.) This ability can be traced back to (i) the kinetic-based fluxes (Eq. (10)) and (ii) the moment-inversion algorithm that generates a realizable velocity distribution function.

[4] By definition, $R^0_{000} = \rho$ and $R^1_{ijk} = 0$.

3. A high-order moment-inversion algorithm

3.1. Quadrature-based moment methods

In quadrature-based moment methods the velocity distribution function is represented by a set of point measures [17]:

$$f(\mathbf{v}) = \sum_{\alpha=1}^{N} \rho_\alpha \delta(\mathbf{v} - \mathbf{U}_\alpha), \tag{14}$$

where the weights ρ_α and velocity abscissas $\mathbf{U}_\alpha$ are uniquely determined from a finite set of moments [17,45]. In our previous work [21], we presented a moment-inversion algorithm for computing the weights and abscissas with $N = 8$ that uses velocity moments up to third order. We also demonstrated that the resulting flow code could be used to approximate flows with arbitrary Knudsen number. However, due to the relatively low order of the moments employed, the accuracy of the flow predictions decreases (except in very particular cases such as two crossing jets without collisions) with increasing Knudsen number. Thus, in order to improve the accuracy for larger Knudsen numbers, we seek to increase the order of the moments used in the quadrature or, equivalently, to increase the number of abscissas.

In terms of the quadrature weights ρ_α and abscissas $\mathbf{R}_\alpha = (r_{1\alpha}, r_{2\alpha}, r_{3\alpha})$, the rotated central moments can be expressed as

$$R^{\gamma}_{ijk} = \sum_{\alpha=1}^{N} \rho_\alpha r^i_{1\alpha} r^j_{2\alpha} r^k_{3\alpha}. \tag{15}$$

Note that for moments in the moment set used to construct the quadrature, this expression is exact. For all other moments, Eq. (15) is the quadrature approximation for R^{γ}_{ijk}. By replacing $\mathbf{R}_\alpha$ with $\mathbf{U}_\alpha$, an expression analogous to Eq. (15) can be written for the moments M^{γ}_{ijk}. Likewise, the flux vectors in Eq. (10) can be written using Eq. (14) as

$$\begin{aligned} Q^{-}_{n,ijk} &= \sum_{\alpha=1}^{N} \rho_\alpha \min(u_{n\alpha}, 0) u^i_{1\alpha} u^j_{2\alpha} u^k_{3\alpha}, \\ Q^{+}_{n,ijk} &= \sum_{\alpha=1}^{N} \rho_\alpha \max(u_{n\alpha}, 0) u^i_{1\alpha} u^j_{2\alpha} u^k_{3\alpha}, \end{aligned} \tag{16}$$

where $\mathbf{U}_\alpha = (u_{1\alpha}, u_{2\alpha}, u_{3\alpha})$. In this work, we are primarily interested in determining how the accuracy of Eq. (16) depends on the order of the quadrature approximation (or, equivalently, on the choice for N).

In the following, the steps used to construct the quadrature will be the same for each n:

(1) Using $2n$ moments in each direction (e.g. $R^0_{000}, R^1_{001}, \ldots, R^{2n-1}_{002n-1}$), compute n univariate weights and n abscissas using the product-difference (PD) algorithm [29,45,52,61] (see Appendix A).
(2) Construct the velocity abscissas $\mathbf{R}_\alpha$ from the tensor product of the abscissas in each direction.
(3) Compute the weights ρ_α by solving a linear system formed from the set of mixed moments with indices up to $n-1$ (e.g. $R^2_{110}, R^2_{101}, \ldots, R^{3n-3}_{n-1n-1n-1}$).

For the 1-D quadratures in step (1), the weights from the PD algorithm are guaranteed to be non-negative for realizable moments, and the abscissas will be highly nonlinear functions of the $2n$ moments [17,29,61]. The question of whether or not the resulting 3-D quadrature is valid depends on the final step. If the weights are non-negative, then the reconstructed distribution function (Eq. (14)) will be realizable. The latter is particularly important because of the kinetic scheme used to compute the fluxes (Eq. (16)). Indeed, the overall numerical scheme will only be stable if the fluxes are defined using a realizable distribution function. For Maxwellian distributions, the quadratures computed using the above steps will always have positive weights (i.e. they will correspond to Gauss–Hermite quadratures [56]). As the moments used to construct the quadrature move farther away from the Maxwellian values, it is possible for one or more of the weights to be become negative.[5] In previous work [21], we showed that for 8-node quadrature it is possible to eliminate the negative weight by setting it to zero and reducing the size of the linear system in step (3). However, in actual calculations with 8-node quadrature we found that this procedure was never needed. Likewise, for the Riemann shock problem considered in this work, we do not observe negative weights for any of the quadratures. However, it is possible to select realizable moments that generate one or more negative weights. In general, an algorithm will be needed to "deflate" the linear system in step (3) by setting negative weights to zero and solving a reduced linear system for the remaining weights. However, such an algorithm is likely to be somewhat complicated in order to deal with each special case (e.g. one vs. multiple zero weights). We will thus leave construction of an algorithm to deal with negative weights to future work.

Concerning the order of the quadrature, there are three possible choices: (i) the order of the highest moment used to construct the quadrature ($\gamma = 3n-3$), (ii) the order of the highest moment used in the univariate quadrature ($\gamma = 2n-1$), or (iii) the highest order for which all moments of that order are included ($\gamma = n$). For univariate quadrature, the abscissas found

[5] Experience shows that this is more likely to occur with inelastic collisions or near boundary with specular reflections.

from the PD algorithm are the zeros of an orthogonal polynomial of order n [17,29,61]. For example, if the moments correspond to a standardized Gaussian distribution, then the abscissas will be the Gauss–Hermite quadrature points [56]. In comparison to lattice Boltzmann methods with fixed discrete velocities and varying weights where the formal order in one dimension is determined by the number of abscissas (n) [35], by allowing both the weights and abscissas to vary the quadrature method of moments in one dimension doubles the order the accuracy [17,45]. Hereinafter, since there is ambiguity as to the order, we will refer to each quadrature by the number of nodes in velocity phase space (i.e. n^3).

For completeness, we note that the simplest quadrature uses one node and controls only the first four moments (i.e. $\rho, \mathbf{U}$), resulting in the pressure-less gas dynamics equation [5,6,11]. In most applications, the second-order moments are important and thus we will consider only quadratures with $n > 1$. Moreover, because 2-D quadratures can be found from 3-D quadratures by eliminating the moments in the third direction, in the following we will only discuss construction of quadratures for 3-D cases. For completeness, we will begin by reviewing the 8-node quadrature developed in [21].

3.2. 8-Node quadrature

An 8-node quadrature can be constructed using the following set of 14 moments (including only four of the ten third-order moments):[6]

$$\left(R^0_{000}, R^1_{100}, R^1_{010}, R^1_{001}, R^2_{200}, R^2_{110}, R^2_{101}, R^2_{020}, R^2_{011}, R^2_{002}, R^3_{300}, R^3_{111}, R^3_{030}, R^3_{003}\right).$$

The abscissas are constructed from the tensor product of the univariate abscissas in each of the three directions [21]. Let $X_{(i)1}$ and $X_{(i)2}$ denote the two abscissas in direction $i \in (1,2,3)$, and $\rho_{(i)1}$ and $\rho_{(i)2}$ the corresponding weights. By applying the PD algorithm, we find

$$\begin{aligned}
&\left(R^0_{000}, R^1_{100}, R^2_{200}, R^3_{300}\right) \Rightarrow (\rho_{(1)1}, \rho_{(1)2}, X_{(1)1}, X_{(1)2}),\\
&\left(R^0_{000}, R^1_{010}, R^2_{020}, R^3_{030}\right) \Rightarrow (\rho_{(2)1}, \rho_{(2)2}, X_{(2)1}, X_{(2)2}),\\
&\left(R^0_{000}, R^1_{001}, R^2_{002}, R^3_{003}\right) \Rightarrow (\rho_{(3)1}, \rho_{(3)2}, X_{(3)1}, X_{(3)2}).
\end{aligned} \tag{17}$$

Using the tensor product, the set of eight abscissas $\mathbf{R}_\alpha$ is given by

$$\begin{aligned}
&\{(X_{(1)1}, X_{(2)1}, X_{(3)1}), (X_{(1)2}, X_{(2)1}, X_{(3)1}),\\
&(X_{(1)1}, X_{(2)2}, X_{(3)1}), (X_{(1)2}, X_{(2)2}, X_{(3)1}),\\
&(X_{(1)1}, X_{(2)1}, X_{(3)2}), (X_{(1)2}, X_{(2)1}, X_{(3)2}),\\
&(X_{(1)1}, X_{(2)2}, X_{(3)2}), (X_{(1)2}, X_{(2)2}, X_{(3)2})\},
\end{aligned} \tag{18}$$

which uniquely determines the velocity abscissas $\mathbf{U}_\alpha$ using Eq. (13).

As noted earlier, the weights ρ_α are determined by solving a linear system. The first four equations in the linear system are found by enforcing agreement with the three univariate quadratures:

$$\begin{aligned}
\rho_1 + \rho_3 + \rho_5 + \rho_7 &= \rho_{(1)1},\\
\rho_2 + \rho_4 + \rho_6 + \rho_8 &= \rho_{(1)2},\\
\rho_1 + \rho_2 + \rho_5 + \rho_6 &= \rho_{(2)1},\\
\rho_1 + \rho_2 + \rho_3 + \rho_4 &= \rho_{(3)1}.
\end{aligned} \tag{19}$$

The remaining four equations are found by enforcing the mixed moments:[7]

$$\begin{aligned}
&X_{(1)1}X_{(2)1}\rho_1 + X_{(1)2}X_{(2)1}\rho_2 + X_{(1)1}X_{(2)2}\rho_3 + X_{(1)2}X_{(2)2}\rho_4 + X_{(1)1}X_{(2)1}\rho_5 + X_{(1)2}X_{(2)1}\rho_6 + X_{(1)1}X_{(2)2}\rho_7 + X_{(1)2}X_{(2)2}\rho_8 = R^2_{110},\\
&X_{(1)1}X_{(3)1}\rho_1 + X_{(1)2}X_{(3)1}\rho_2 + X_{(1)1}X_{(3)1}\rho_3 + X_{(1)2}X_{(3)1}\rho_4 + X_{(1)1}X_{(3)2}\rho_5 + X_{(1)2}X_{(3)2}\rho_6 + X_{(1)1}X_{(3)2}\rho_7 + X_{(1)2}X_{(3)2}\rho_8 = R^2_{101},\\
&X_{(2)1}X_{(3)1}\rho_1 + X_{(2)1}X_{(3)1}\rho_2 + X_{(2)2}X_{(3)1}\rho_3 + X_{(2)2}X_{(3)1}\rho_4 + X_{(2)1}X_{(3)2}\rho_5 + X_{(2)1}X_{(3)2}\rho_6 + X_{(2)2}X_{(3)2}\rho_7 + X_{(2)2}X_{(3)2}\rho_8 = R^2_{011},\\
&X_{(1)1}X_{(2)1}X_{(3)1}\rho_1 + X_{(1)2}X_{(2)1}X_{(3)1}\rho_2 + X_{(1)1}X_{(2)2}X_{(3)1}\rho_3 + X_{(1)2}X_{(2)2}X_{(3)1}\rho_4 + X_{(1)1}X_{(2)1}X_{(3)2}\rho_5 + X_{(1)2}X_{(2)1}X_{(3)2}\rho_6\\
&\quad + X_{(1)1}X_{(2)2}X_{(3)2}\rho_7 + X_{(1)2}X_{(2)2}X_{(3)2}\rho_8 = R^3_{111},
\end{aligned} \tag{20}$$

which follow directly from the definition of the rotated central moments in terms of the quadrature weights and abscissas (Eq. (15)). This system of equations can be solved to find the weights. As discussed in [21], the weights will be non-negative as long as R^3_{111} is close to zero. As mentioned earlier, in all applications of 8-node quadrature carried out to date, the weights have remained non-negative.

[6] For consistency, we will always list moments in the order determined by decreasing the ith index, then the jth index, and finally the kth index for a given order.

[7] Recall that by definition $R^2_{110} = R^2_{101} = R^2_{011} = 0$. The left-hand side of these equations is simply Eq. (15) with the abscissas $(r_{1\alpha}, r_{2\alpha}, r_{3\alpha})$ replaced by Eq. (18).

Table 1
Order and indices for 36 rotated central moments R^{γ}_{ijk} in 27-node quadrature.

γ	0	1	1	1	2	2	2	2	2	2	3	3	3	3	3	3	3	3	3	3
i	0	1	0	0	2	1	1	0	0	0	3	2	2	1	1	1	0	0	0	0
j	0	0	1	0	0	1	0	2	1	0	0	1	0	2	1	0	3	2	1	0
k	0	0	0	1	0	0	1	0	1	2	0	0	1	0	1	2	0	1	2	3
γ	4	4	4	4	4	4	4	4	4	5	5	5	5	5	5	6				
i	4	2	2	2	1	1	0	0	0	5	2	2	1	0	0	2				
j	0	2	1	0	2	1	4	2	0	0	2	1	2	5	0	2				
k	0	0	1	2	1	2	0	2	4	0	1	2	2	0	5	2				

3.3. Extension to n^3-node quadrature

Before discussing n^3-node quadrature, a few remarks on the 8-node quadrature will prove insightful. First, we note from Eq. (19) that in direction 1 two equations are needed to control $\rho_{(1)1}$ and $\rho_{(1)2}$, while only one equation is needed in the other two directions. (The other two equations are linearly dependent [21].) In general, n equations will result for direction 1 and $n-1$ equations for each of the other two directions. The total number of linear equations that is found by enforcing the three univariate quadratures is thus $N_1 = 3n-2$. The remaining $N_2 = n^3 - 3n + 2$ linear equations come from fixing the mixed moments. Second, the selection of the mixed moments cannot be done arbitrarily. At a minimum, for a particular mixed moment the resulting equation must be linearly independent. The choice of mixed moments with indices less than or equal to $n-1$ ensures that the linear system is non-singular and, because the number of such moments equals N_2, appears to be unique. Although we do not have a proof for the latter, experience with Maxwellian moments [22] suggests that replacing any one of these mixed moments with another one not included in the set results in a singular system. Third, the N_1 equations found by enforcing the univariate quadratures can be replaced by the N_1 non-mixed moment equations up to order $n-1$ (e.g., $R^0_{000}, R^1_{100}, R^1_{010}, R^1_{001}$ for $n=2$). This follows from the fact that the 1-D quadratures exactly reproduce these moments.[8] In summary, the quadrature weights can be determined from a linear system involving the n^3 moments with indices $n-1$ or less.

Based on the observations given above, we can conclude that the total number of moments needed to define the n^3-node quadrature is $N_3 = (n^2+3)n$. Hence, the input to the moment-inversion algorithm is the set of N_3 moments R^{γ}_{ijk} with $0 \leqslant i,j,k < n$ and $R^i_{i00}, R^j_{0j0}, R^k_{00k}$ with $n \leqslant i,j,k < 2n$. For $n=3$, the resulting 27-node quadrature requires 36 moments (see Table 1). For $n=4$, the 64-node quadrature uses 76 moments (see Table 2). We have successfully implemented the moment-inversion algorithm to construct n^3-node quadratures for $n \leqslant 4$ in 3-D, and n^2-node quadratures for $n \leqslant 5$ in 2-D. Implementation for larger n is hindered only by practical considerations concerning the number of moment transport equations that must be solved. In all cases investigated thus far the linear system used to find the weights remained well conditioned. Our numerical implementation was verified by applying it to Maxwellian moments and checking that the resulting weights and abscissas correspond to Gauss–Hermite quadrature [35,56]. In most of the numerical examples that we have investigated to date, the moments have evolved to values far from Maxwellian without incurring negative weights. However, for flows with very large (or infinite) Knudsen number and specular reflections at the boundaries, negative weights have been observed. For such flows it will be necessary to implement correction algorithms such as the one developed for 8-node quadrature [21].

In conclusion, we should note that the moment-inversion algorithm described above can be used to invert the central moments $\left(C^{\gamma}_{ijk}\right)$ in place of the rotated central moments $\left(R^{\gamma}_{ijk}\right)$ for cases where the velocity covariances are not too large (e.g., low-Mach-number flows such as plane Couette and Poiseuille flows [35]).[9] The advantage of using central moments is that their transport equations are relatively easy to derive [57], while those for rotated central moments are more complicated. In this work we will consider only the Riemann shock problem for which the correlation coefficients are zero (i.e. $R^{\gamma}_{ijk} = C^{\gamma}_{ijk}$). However, in work to be reported elsewhere, we have applied the moment-inversion algorithm with central moments to low-Mach-number flows and find results completely consistent with higher-order lattice Boltzmann methods [35]. Another approach [21] is to transport the moments M^{γ}_{ijk} and use a projection to recompute them using the weights and abscissas at the end of each time step. Because the rotation step couples all central moments of the same order, transporting the moments (or the central moments) requires all moments up to order $3n-3$ (which are needed to compute $R^{3n-3}_{n-1n-1n-1}$). For example, with $n=4$ all 220 moments[10] up to order $\gamma = 9$ must be transported, compared to the 76 rotated central moments needed to compute the weights and abscissas. Thus, a relatively large reduction in the number of moment transport equations could be achieved by solving directly for R^{γ}_{ijk}. Another nontrivial consideration in the numerical implementation is that computing R^{γ}_{ijk} from M^{γ}_{ijk} can be subject to severe round-off errors in cases where the mean velocity $\mathbf{U}$ is large relative to the RMS velocity. In contrast, the computation of R^{γ}_{ijk} from C^{γ}_{ijk} is well behaved.

[8] As noted earlier, negative weights cannot be caused by non-mixed moments. Thus, any correction algorithm designed to eliminate negative weights must rely on removing mixed moments.

[9] For Gaussian moments, the weights will be non-negative if the magnitudes of the correlation coefficients are less than approximately 0.5.

[10] The number of moments of order γ in 3-D is $(\gamma+1)(\gamma+2)/2$.

Table 2
Order and indices for 76 rotated central moments R^{γ}_{ijk} in 64-node quadrature.

γ	0	1	1	1	2	2	2	2	2	2	3	3	3	3	3	3	3	3	3	3
i	0	1	0	0	2	1	1	0	0	0	3	2	2	1	1	1	0	0	0	0
j	0	0	1	0	0	1	0	2	1	0	0	1	0	2	1	0	3	2	1	0
k	0	0	0	1	0	0	1	0	1	2	0	0	1	0	1	2	0	1	2	3
γ	4	4	4	4	4	4	4	4	4	4	4	4	4	4	4	5	5	5	5	5
i	4	3	3	2	2	2	1	1	1	1	0	0	0	0	0	5	3	3	3	2
j	0	1	0	2	1	0	3	2	1	0	4	3	2	1	0	0	2	1	0	3
k	0	0	1	0	1	2	0	1	2	3	0	1	2	3	4	0	0	1	2	0
γ	5	5	5	5	5	5	5	5	5	5	6	6	6	6	6	6	6	6	6	6
i	2	2	2	1	1	1	0	0	0	0	6	3	3	3	3	2	2	2	1	1
j	2	1	0	3	2	1	5	3	2	0	0	3	2	1	0	3	2	1	3	2
k	1	2	3	1	2	3	0	2	3	5	0	0	1	2	3	1	2	3	2	3
γ	6	6	6	7	7	7	7	7	7	7	7	7	8	8	8	9				
i	0	0	0	7	3	3	3	2	2	1	0	0	3	3	2	3				
j	6	3	0	0	3	2	1	3	2	3	7	0	3	2	3	3				
k	0	3	6	0	1	2	3	2	3	3	0	7	2	3	3	3				

4. Numerical algorithm for moment transport

For the applications considered in Section 5, the rotated central moments are the same as the central moments. Moreover, the mean velocity is at most only a factor of two larger than the RMS velocity (i.e. the speed of sound). We will thus work directly with the moments M^{γ}_{ijk}. The system of moment transport equations (Eq. (6)) can be solved numerically for 3-D problems by extending the numerical methods described in [15,16,21]. Here, however, we are interested in shock propagation in only one spatial dimension and time. Hence we will describe the numerical method in the context of one-dimensional fluxes. The algorithm follows closely to the one described in [21] with modifications to increase the order of the time and space discretizations. Although the body force term is not required for the Riemann shock problem, we will include it in the discussion here for future use (i.e. finite-Stokes-number flows).

4.1. Notation and moment transport equation

Let x_1 be the inhomogeneous direction and $-x_2$ be the direction of the body force. The vector of moments will be denoted by $\mathbf{M} = \left[M^{\gamma}_{ijk}\right]$, where each component corresponds to a particular set of i, j, k. The corresponding set of weights and abscissas found from the moment-inversion algorithm will be denoted by $\mathbf{N} = [\rho_\alpha, \mathbf{U}_\alpha]$. The vector of equilibrium moments will be denoted by $\mathbf{\Delta} = \left[\Delta^{\gamma}_{ijk}\right]$. The vectors of the two components of the spatial fluxes in the direction x_1, which are functions of $\mathbf{N}$ (Eq. (16)), will be denoted by $\mathbf{Q}^{-}_1(\mathbf{N}) = \left[Q^{-}_{1,ijk}\right]$ and $\mathbf{Q}^{+}_1(\mathbf{N}) = \left[Q^{+}_{1,ijk}\right]$. The vector of moments appearing in the body force term, which is a subset of $\mathbf{M}$, will be denoted by $\mathbf{M}_g = \left[jM^{\gamma-1}_{ij-1k}\right]$. Using this notation, the one-dimensional moment transport equation becomes

$$\partial_t \mathbf{M} + \partial_{x_1}\left(\mathbf{Q}^{-}_1(\mathbf{N}) + \mathbf{Q}^{+}_1(\mathbf{N})\right) = -g\mathbf{M}_g + \frac{1}{\tau}(\mathbf{\Delta} - \mathbf{M}). \tag{21}$$

Note that $\mathbf{\Delta}$ depends on the lower-order moments through $\rho, \mathbf{U}$ and σ_{eq}. In most applications, τ will depend on ρ and σ_{eq}. The moment transport equation will be solved using a kinetic-based finite-volume method [16,21]. Note, however, that when designing such an algorithm care must be taken to ensure that the moment set remains realizable when advanced in time (in particular during the spatial transport step [46,60,63]). In quadrature-based moment methods, realizable moments are required for the moment-inversion algorithm.

4.2. The solution algorithm

In previous work [21], a first-order algorithm was proposed. Here, we develop an algorithm that uses a modified two-step Runga-Kutta method for advancing in time and a second-order flux-limited method in space. In order to accommodate the various physical processes, time splitting is used inside each Runga-Kutta step. We will use the subscript $_\Delta$ to denote quantities evaluated at the half-time step. The time step Δt is adjusted on each iteration to account for changes in the velocity abscissas and the collision frequency. The solution is obtained on a fixed uniform grid of size Δx. For the Riemann shock problem, the boundary conditions are not important if the shocks are not allowed to reach the boundaries. We will thus use the reflective boundaries described in [21]. For initial conditions, the moments in the entire computational domain are set to Maxwellian with local values for the density, mean velocity, and particle temperature. The initial conditions for the Riemann shock problem are as follows: the density changes from ρ_l to ρ_r at the centerline, the mean velocity is null, and the particle temperature is uniform (set equal to unity).

The individual steps in the solution algorithm are as follows:

(1) Initialize moments $\mathbf{M}$.
(2) Compute central moments from $\mathbf{M}$ and use the moment-inversion algorithm to compute $\mathbf{N}$.
(3) Advance the moments in time by Δt using the moment transport equations:
  (a) Evaluate Δt.
  (b) Set $\mathbf{M}_\Delta = \mathbf{M}$.
  (c) Evaluate moments and weights and abscissas at half-time step (time split):
    (i) Advance $\mathbf{M}_\Delta$ by $\Delta t/2$ due to spatial fluxes $\mathbf{Q}_1^-(\mathbf{N})$ and $\mathbf{Q}_1^+(\mathbf{N})$.
    (ii) Compute central moments from $\mathbf{M}_\Delta$ and use the moment-inversion algorithm to compute $\mathbf{N}_\Delta$.
    (iii) Advance $\mathbf{N}_\Delta$ and $\mathbf{M}_\Delta$ by $\Delta t/2$ due to body forces.
    (iv) Advance $\mathbf{M}_\Delta$ by $\Delta t/2$ due to collisions.
    (v) Compute central moments from $\mathbf{M}_\Delta$ and use the moment-inversion algorithm to compute $\mathbf{N}_\Delta$.
    (vi) Apply boundary conditions to $\mathbf{M}_\Delta$ and $\mathbf{N}_\Delta$.

  (d) Advance moments and weights and abscissas for full time step (time split):
    (i) Advance $\mathbf{M}$ by Δt due to spatial fluxes $\mathbf{Q}_1^-(\mathbf{N}_\Delta)$ and $\mathbf{Q}_1^+(\mathbf{N}_\Delta)$.
    (ii) Compute central moments from $\mathbf{M}$ and use the moment-inversion algorithm to compute $\mathbf{N}$.
    (iii) Advance $\mathbf{N}$ and $\mathbf{M}$ by Δt due to body forces.
    (iv) Advance $\mathbf{M}$ by Δt due to collisions.

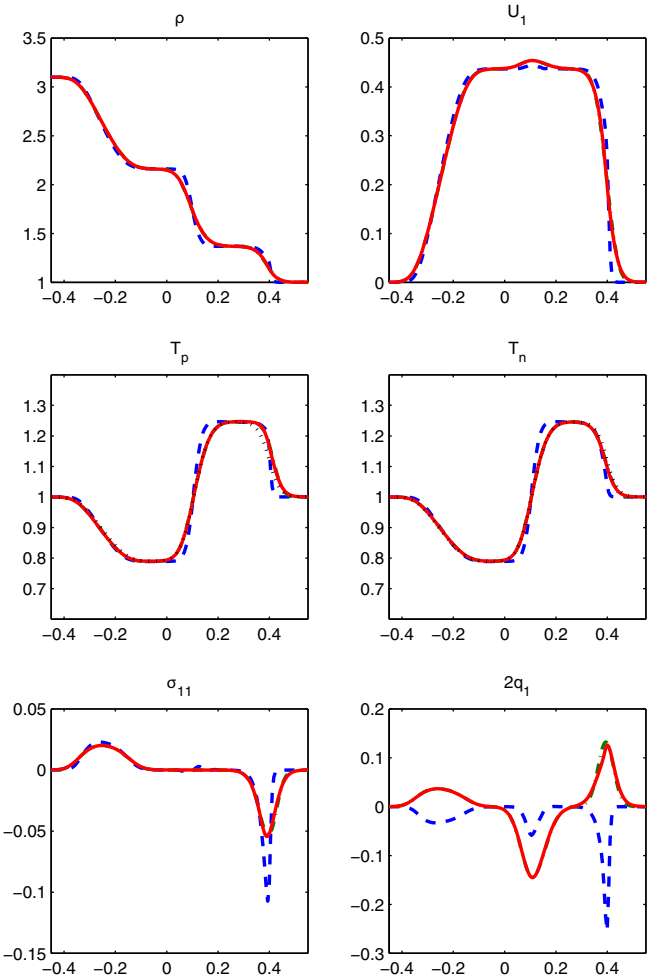

Fig. 1. Selected moments for the Riemann shock problem with $Ma = 1.25$ and $\beta = 0.01$ at $t = 0.307$. Dashed line (blue): 8-node quadrature. Dash-dot line (green): 27-node quadrature. Solid line (red): 64-node quadrature. Dotted line (black): Particle temperature. (For interpretation of the references in colour in this figure legend, the reader is referred to the web version of this article.)

(v) Compute central moments from **M** and use the moment-inversion algorithm to compute **N**.
(vi) Apply boundary conditions to **M** and **N**.

(4) Return to step 3.

In the inner most loops (3c) and (3d), the moments are advanced sequentially (i.e. time splitting) with the output from a sub-step used to evaluate the change in the next sub-step. The details on each of the sub-steps are described next. Note that in order to keep the notation as simple as possible, we do not introduce new symbols to indicate the values of **M** at the end of each sub-step. Instead, we let $\mathbf{M}^*$ denote the value of the moments at the end of a sub-step (and thus implicitly at the beginning of the next sub-step).

4.2.1. Time-step evaluation

The time step Δt is set to a fraction of the smallest characteristic time (advection or collisions):

$$\Delta t = \min(\tau/10, \tau_{\mathrm{CFL}}) \tag{22}$$

where τ and τ_{CFL} are, respectively, the smallest local collision and advection times in the entire domain at the current time step. For each grid cell, the local advection time is defined by

$$\tau_{\mathrm{CFL}} = C_{\mathrm{CFL}} \Delta x / U_{\max} \tag{23}$$

where $U_{\max} = \max_\alpha |u_{1\alpha}|$ and $u_{1\alpha}$ are the local u_1-velocity abscissas. In the Riemann shock problem, the Courant number C_{CFL} is set to 0.5, and we define the local collision time as

$$\tau = \frac{\beta}{\rho \sqrt{\sigma_{\mathrm{eq}}}} \tag{24}$$

where β (proportional to the collision cross section) is a constant. Note that the Knudsen number varies linearly with β.

4.2.2. Spatial fluxes

Because of the conservative form of Eq. (21), the finite-volume method [40] is a natural candidate for its discretization. The underlying kinetic equation (Eq. (1)) can be used for the derivation of a numerical flux formula that ensures the robustness of the corresponding scheme. The finite-volume scheme used in this work to advance by Δt the moments at grid cell i is defined by

$$\mathbf{M}_i^* = \mathbf{M}_i - \frac{\Delta t}{\Delta x}\left[\mathbf{G}_1\left(\mathbf{N}_i^+, \mathbf{N}_{i+1}^-\right) - \mathbf{G}_1\left(\mathbf{N}_{i-1}^+, \mathbf{N}_i^-\right)\right], \tag{25}$$

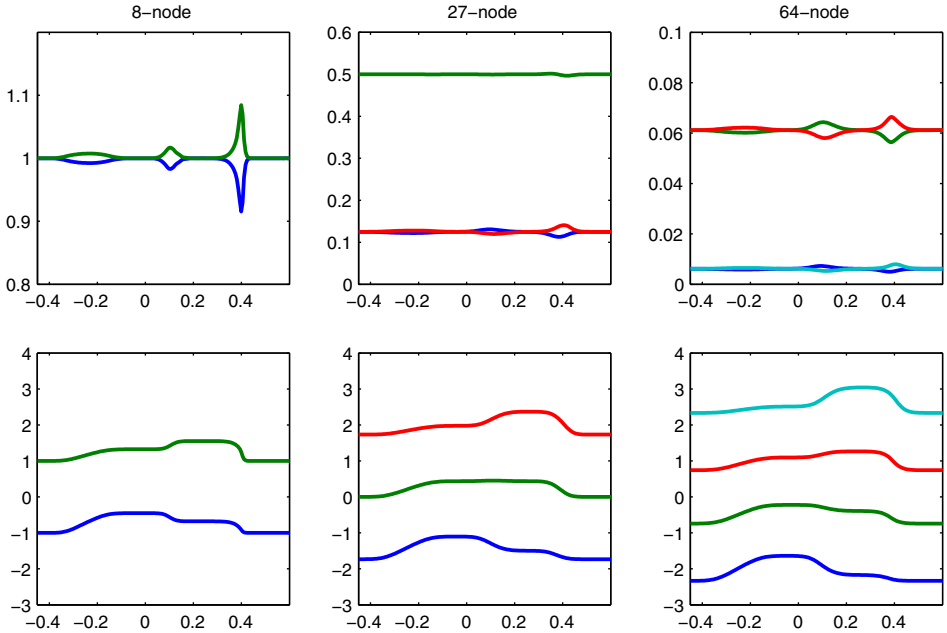

Fig. 2. Normalized weights (top) and u_1-velocity abscissas (bottom) for the Riemann shock problem with $Ma = 1.25$ and $\beta = 0.01$ at $t = 0.307$.

where $\mathbf{G}_1$ is the flux function defined in terms of the weights and abscissas (Eq. (16)):

$$\mathbf{G}_1(\mathbf{N}^+, \mathbf{N}^-) = \mathbf{Q}_1^+(\mathbf{N}^+) + \mathbf{Q}_1^-(\mathbf{N}^-). \tag{26}$$

In the first-order scheme used in our previous work [16], $\mathbf{N}^+ = \mathbf{N}^- = \mathbf{N}$. More generally, in order to be consistent with the kinetic-based description of the fluxes (Eq. (10)), $\mathbf{Q}_1^+(\mathbf{N}_i^+)$ should be found from the reconstructed velocity distribution function on the right face of grid cell i. Likewise, $\mathbf{Q}_1^-(\mathbf{N}_i^-)$ should be found from the reconstructed velocity distribution function on the left face of grid cell i.

For the second-order scheme, we use the spatial derivatives of the weights and abscissas (denoted by $\partial_1\mathbf{N}$) to evaluate the weights and abscissas at the cell faces (i.e. to reconstruct the velocity distribution function at the cell faces):

$$\begin{aligned} \mathbf{N}^- &= \mathbf{N} - \tfrac{\Delta x}{2}\partial_1\mathbf{N}, \\ \mathbf{N}^+ &= \mathbf{N} + \tfrac{\Delta x}{2}\partial_1\mathbf{N}, \end{aligned} \tag{27}$$

where $\partial_1\mathbf{N}_i$ is defined by

$$\partial_1\mathbf{N}_i = \text{minmod}\left(\frac{\mathbf{N}_i - \mathbf{N}_{i-1}}{\Delta x}, \frac{\mathbf{N}_{i+1} - \mathbf{N}_i}{\Delta x}\right) \tag{28}$$

and

$$\text{minmod}(x, y) = \text{sign}(x)\left(\frac{1 + \text{sign}(xy)}{2}\right)\min(|x|, |y|). \tag{29}$$

In Eq. (28) the minmod function is applied to each component of $\mathbf{N}$.) Note that the first-order scheme is guaranteed [16] to generate realizable moments from Eq. (25). A necessary, although probably not sufficient, condition for obtaining realizable moments from the second-order scheme is that the weights in $\mathbf{N}^-$ and $\mathbf{N}^+$ be non-negative (given that the weights in $\mathbf{N}$ are

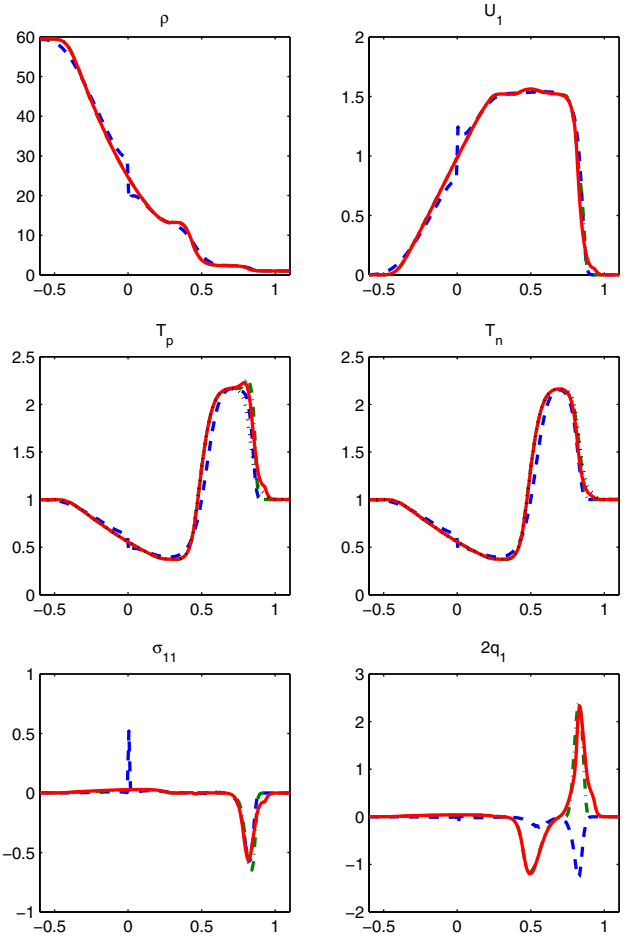

Fig. 3. Selected moments for the Riemann shock problem with $Ma = 2.05$ and $\beta = 0.02$ at $t = 0.307$. Dashed line (blue): 8-node quadrature. Dash-dot line (green): 27-node quadrature. Solid line (red): 64-node quadrature. Dotted line (black): Particle temperature. (For interpretation of the references in colour in this figure legend, the reader is referred to the web version of this article.)

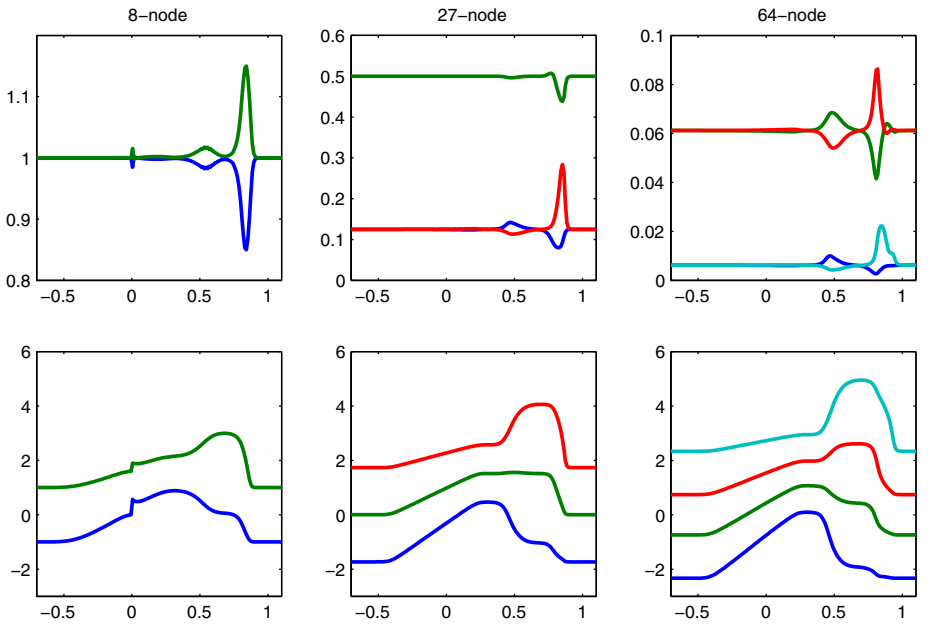

Fig. 4. Normalized weights (top) and u_1-velocity abscissas (bottom) for the Riemann shock problem with $Ma = 2.05$ and $\beta = 0.02$ at $t = 0.307$.

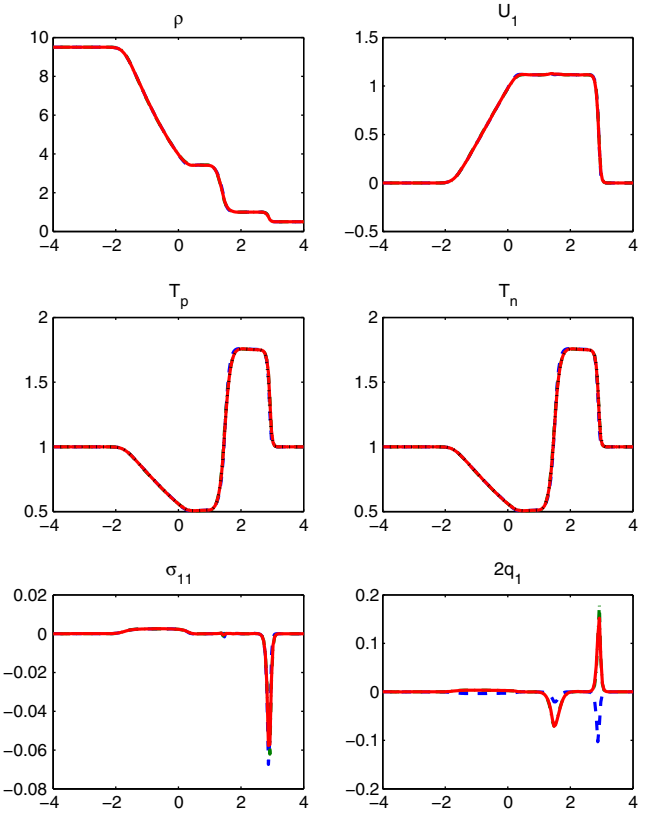

Fig. 5. Riemann shock problem at $t = 1.3$ with $\beta = 0.005$. Dashed line (blue): 8-node quadrature. Dash-dot line (green): 27-node quadrature. Solid line (red): 64-node quadrature. Dotted line (black): Particle temperature. (For interpretation of the references in colour in this figure legend, the reader is referred to the web version of this article.)

non-negative). In other words, the reconstructed velocity distribution functions must be well defined. Note that in previous work [16], the second-order scheme was defined by estimating the moments (i.e. **M** instead of **N**) at the cell faces. Either

method can work, but when using **M** it is more difficult to determine whether the estimated moments are realizable. In contrast, when using **N** it suffices to check that the estimated weights are non-negative. More details on recent advances in the development of higher-order realizable schemes can be found in [60].

4.2.3. Body forces

The body-force term in Eq. (21) is equivalent to [21,23]

$$\begin{aligned} &\frac{\mathrm{d}\rho_\alpha}{\mathrm{d}t} = 0, \\ &\frac{\mathrm{d}u_{i\alpha}}{\mathrm{d}t} = -g\delta_{i2}b \quad \Longleftrightarrow \quad \partial_t \mathbf{M} = -g\mathbf{M}_g. \end{aligned} \tag{30}$$

Thus, given **N**, the changes in the u_2-velocity abscissas over a time step Δt are

$$u_{2\alpha}^* = u_{2\alpha} - g\Delta t, \tag{31}$$

which yields $\mathbf{N}^*$ and, hence, $\mathbf{M}^*$. For velocity-dependent forces, an expression analogous to Eq. (30) also holds [21,23]. However, because the velocity abscissas found by solving a nonlinear ODE will not be constrained to a tensor product, it is necessary to apply the moment-inversion algorithm to $\mathbf{M}^*$. For velocity-independent forces, this is not required since all of the abscissas are translated uniformly in velocity phase space. For the Riemann shock problem, $g = 0$.

4.2.4. Collisions

The change in the moments due to BGK collisions over a time step Δt can be evaluated explicitly at each grid cell:

$$\mathbf{M}^* = \mathbf{\Delta} + (\mathbf{M} - \mathbf{\Delta})\exp(-\Delta t/\tau) \tag{32}$$

where τ is the local collision time (Eq. (24)) evaluated using **M**.

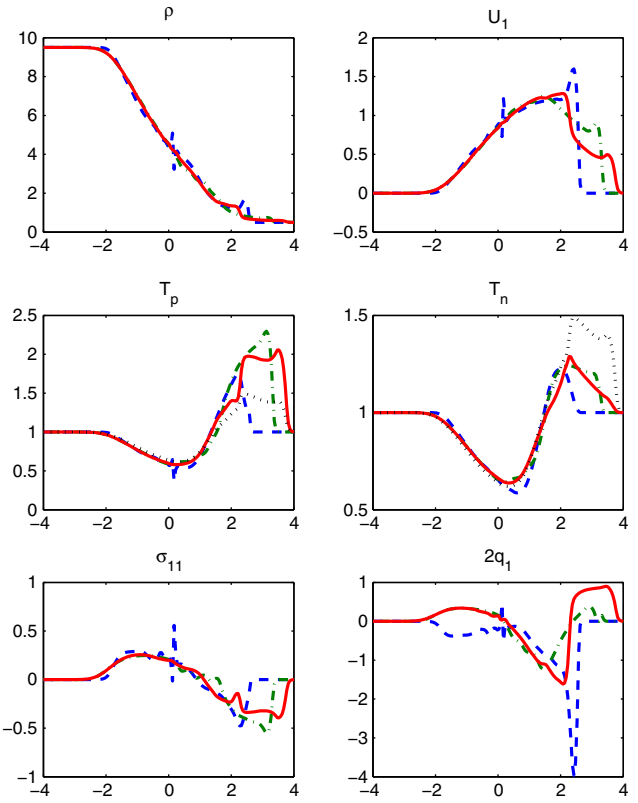

Fig. 6. Riemann shock problem at $t = 1.3$ with $\beta = 0.5$. Dashed line (blue): 8-node quadrature. Dash-dot line (green): 27-node quadrature. Solid line (red): 64-node quadrature. Dotted line (black): Particle temperature. (For interpretation of the references in colour in this figure legend, the reader is referred to the web version of this article.)

5. Application to the Riemann shock problem

In order to test the solution behavior with increasing numbers of nodes, we will simulate the Riemann shock problem in an open domain for different values of the Mach number *Ma* and the Knudsen number *Kn*. Using the initial RMS velocity (i.e. initial particle temperature), the particle diameter, and the number density ρ_r on the right-hand side of the domain, the Boltzmann equation can be made dimensionless. In the Riemann shock problem, the density on the left-hand side of the domain is ρ_l at time zero, and the initial particle temperature is uniform. The velocity distribution function is initially set to Maxwellian with zero mean velocity. The collision time is controlled by the parameter β in Eq. (24). The density ratio ρ_l/ρ_r determines the Mach number. In the limit $\beta = 0$, the moment transport equations reduce to the Euler equation for an inviscid compressible fluid. As discussed in [2,12,50], the time evolution of the system is well known and includes a left-moving rarefaction wave (or expansion fan), a contact surface, and a right-moving shock wave. The velocity of the shock wave in the Euler limit can be computed from the density ratio and the Mach number. When $\beta > 0$ the structure of the solution changes and the temperature in the shock is no longer isotropic. In the absence of collisions ($\beta = \infty$) particles move without changing their velocity. In this work, we are interested in how the solution depends on the number of quadrature nodes for different values of ρ_l/ρ_r and β. Note that, due to the symmetry of the Riemann problem, only a relatively small subset of the transported moments are nonzero (e.g., 24 out of 76 for 64-node quadrature).

In [2], solutions to the Riemann shock problem with $Ma = 1.25$ and $Ma = 2.05$ are presented for finite collision times. Results for $Ma = 1.25$ and $\beta = 0.01$ found using the quadrature-based moment closure with 8, 27, and 64 nodes are presented in Fig. 1. For this case, the collisions are relatively rapid compared to transport, and therefore the particle temperature in the flow direction T_p is only slightly larger than in the normal direction T_n inside the shock. By comparing with the results in [2], we can observe that the 27- and 64-node simulations (which are nearly identical for the quantities shown) are in good agreement, while the 8-node simulation is significantly different. The shear stress σ_{11} and the heat flux q_1 are defined, respectively, in terms of the central moments by

$$\sigma_{11} = \sigma_{eq} - C^2_{200} \quad \text{and} \quad q_1 = \frac{1}{2}\left(C^3_{300} + C^3_{120} + C^3_{102}\right).$$

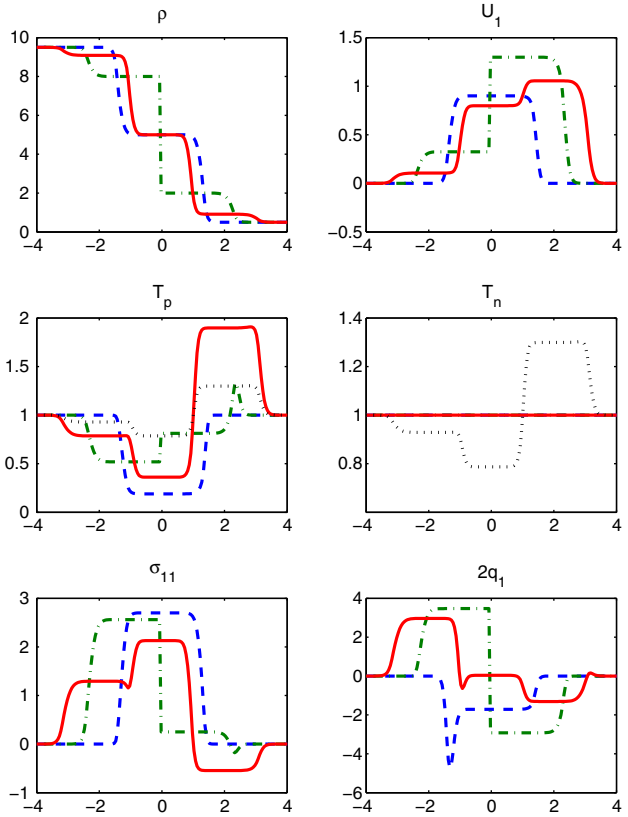

Fig. 7. Riemann shock problem at $t = 1.3$ with $\beta = \infty$. Dashed line (blue): 8-node quadrature. Dash-dot line (green): 27-node quadrature. Solid line (red): 64-node quadrature. Dotted line (black): Particle temperature. (For interpretation of the references in colour in this figure legend, the reader is referred to the web version of this article.)

Note that q_1 contains third-order moments that are not included in the 8-node quadrature (i.e. they are closed using the quadrature), while such moments are included in the 27- and 64-node quadratures. It can be observed from the plots of q_1 in Fig. 1 that the 8-node quadrature predicts the incorrect behavior inside the shock and in the rarefaction wave, and this results in an under prediction of σ_{11} in the shock. In contrast, the 27- and 64-node quadratures predict the correct behavior for σ_{11} and q_1.

In order to understand the structure of the solution for $Ma = 1.25$ as a function of the number of quadrature nodes, we present in Fig. 2 the normalized weights and u_1-velocity abscissas corresponding to Fig. 1. Note that the weights are normalized such that for a Maxwellian distribution they would be independent of position. Thus, the deviations from straight lines observed in Fig. 2 indicate points in the flow where the velocity distribution is not in equilibrium (i.e. due to non-zero β). For $\beta = 0.01$, the deviations are relatively small. The u_1-velocity abscissas in Fig. 2 determine the spatial fluxes in the kinetic-based solver. Each abscissa is governed by a Riemann equation [23] with interaction terms due to collisions. By increasing the number of nodes, the spatial fluxes are described with more characteristic velocities. As noted above, in order to correctly capture q_1 at least three u_1-velocity abscissas are required for $\beta = 0.01$.

The results for $Ma = 2.05$ are shown in Figs. 3 and 4. Consistent with the lower-Mach-number case, we observe that q_1 is not well predicted with 8-node quadrature. Moreover, the error in σ_{11} near the origin generates a discontinuity in ρ and U_1.

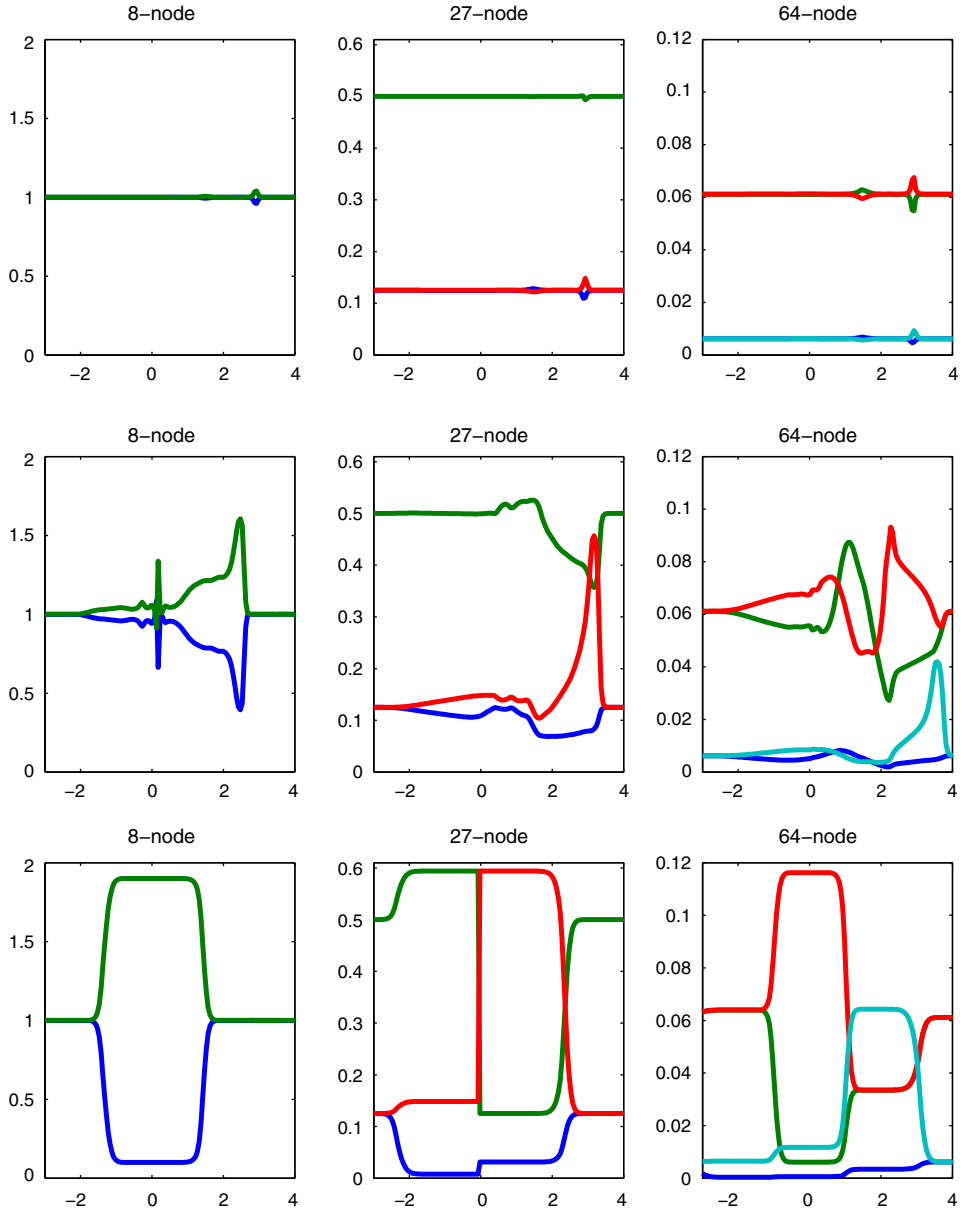

Fig. 8. Normalized weights for Riemann shock problem at $t = 1.3$. Top: $\beta = 0.005$. Middle: $\beta = 0.5$. Bottom: $\beta = \infty$.

From Fig. 4 we see that the discontinuity arises in the 8-node quadrature when the lower u_1-velocity abscissa changes sign from negative to positive. Remarkably, no discontinuities are observed for 27- or 64-node quadrature, even though the u_1-velocity abscissas change sign. For $Ma = 2.05, T_p$ and T_n are relatively far from equilibrium. Comparing the 27- and 64-node quadratures, we see that the results in Fig. 3 are very similar at all locations except inside the shock where the Knudsen number is largest [2]. Thus, as expected, as the Knudsen number increases more quadrature nodes are requires to capture the non-equilibrium behavior. The extent of the latter can be judged by the deviations of the normalized weights in Fig. 4, which are largest just inside the shock.

In order to probe the dependence of the quadrature-based moment method on the Knudsen number, we have computed the Riemann shock problem with $\rho_l/\rho_r = 19$ for three values of β: 0.005, 0.5, and ∞ (i.e. collision-less particles). For all three cases, we initialize the velocity distribution function as Maxwellian with unit particle temperature and zero mean velocity. The case with $\beta = 0.005$ is highly collisional and the results (Fig. 5) are close to the Euler solution. Note that for 8, 27, and 64 nodes the density, mean velocity and particle temperatures are nearly identical. However, as observed earlier, q_1 inside the shock has the wrong sign for 8-node quadrature. This is again a result of not transporting all of the third-order moments in 8-node quadrature. The case with $\beta = 0.5$ is weakly collisional and the results (Fig. 6) are significantly different than the Euler solution. With 8-node quadrature, the discontinuities in the moments are again observed, as well as the poor predictions of

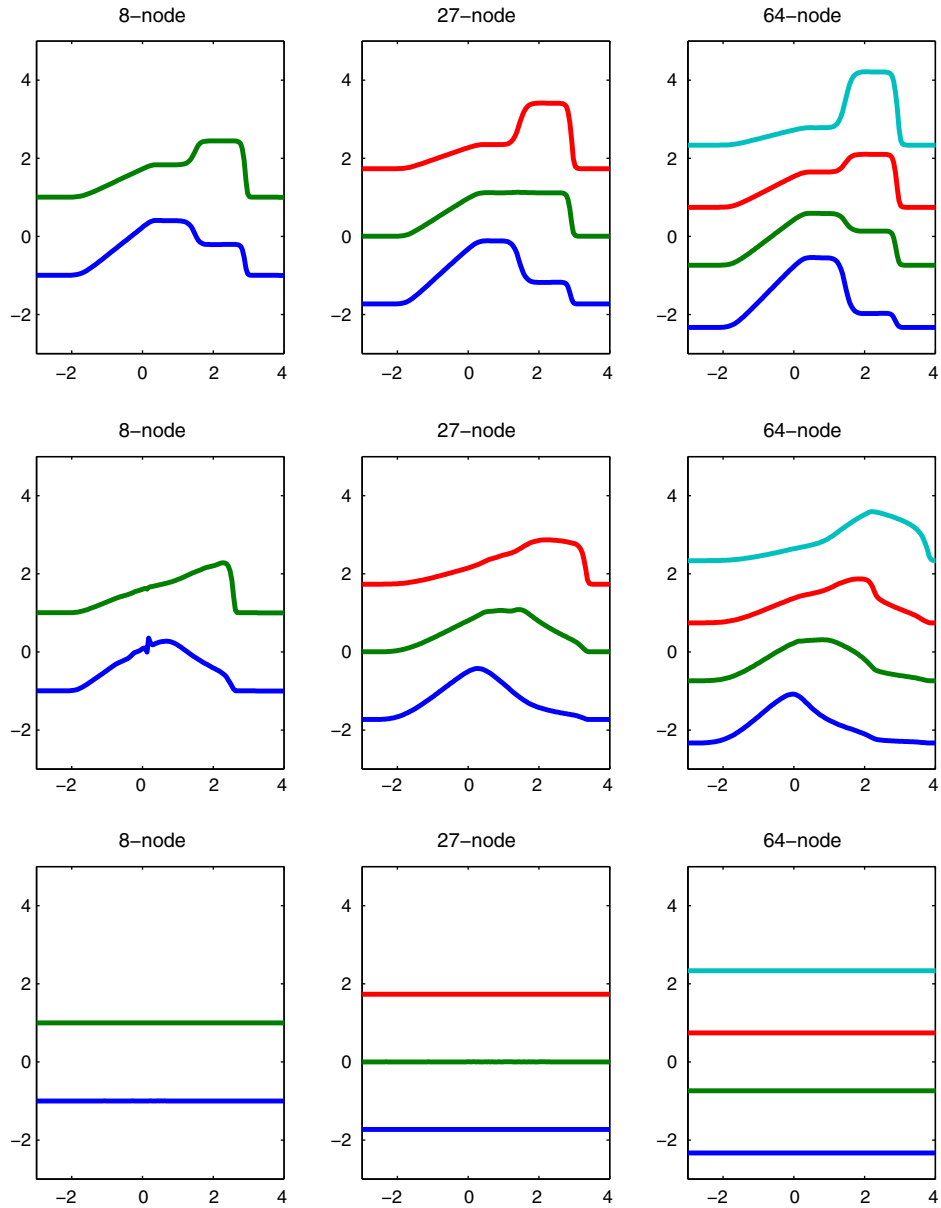

Fig. 9. u_1-velocity abscissas for Riemann shock problem at $t = 1.3$. Top: $\beta = 0.005$. Middle: $\beta = 0.5$. Bottom: $\beta = \infty$.

q_1 in the shock. Behind the shock, the results for 27- and 64-node quadrature are in good agreement, but inside the shock they are very different. This result suggests that more than 64 nodes will be required for weakly collisional flows. The results for collision-less particles are shown in Fig. 7 and, as expected, the results depend strongly on the number of nodes. Nevertheless, despite the lack of collisions, it is noteworthy that the reconstructed distribution function remains realizable (i.e. the weights are positive).

The behavior of the normalized weights and u_1-velocity abscissas are shown in Figs. 8 and 9, respectively, for each value of β and for 8-, 27-, and 64-node quadratures. For $\beta = 0.5$, it is clear that the velocity distribution function is strongly non-equilibrium, especially in the shock. For $\beta = \infty$, the normalized weights change discontinuously, while the u_1-velocity abscissas remain unchanged. As mentioned earlier, the latter is completely consistent with the un-coupled structure of the pressure-less gas dynamics equation that governs each velocity abscissa in the collision-less limit [23]. In this limit, the weights are transported with constant velocities and thus the smooth changes in the weights seen in Fig. 8 for $\beta = \infty$ are due to numerical diffusion. It is remarkable that the u_1-velocity abscissas remain constant for $\beta = \infty$, even though they are computed indirectly by transporting the moments and using the moment-inversion algorithm. This fact demonstrates that the kinetic-based algorithm retains the hyperbolic nature of the abscissa transport equations. Finally, we should note that the solution in the collision-less limit is very dependent on the initial velocity distribution function (which was set to Maxwellian in this work). One could, for example, choose an initial distribution with a finite set of velocities for which the quadrature representation is exact (e.g., the crossing-jets problem considered in [21]). Thus, in general, there will not be a one-to-one correspondence between the number of moments needed to represent a solution to the kinetic equation and value of the Knudsen number.

As a final example, we consider a variation on the Riemann problem where the initial density is uniform, but the RMS velocities are different on the left and right halves of the domain. Unlike in the previous example with uniform temperature, the velocity abscissas will not be constant for $\beta = \infty$. Instead, at time zero the velocity abscissas are discontinuous at the origin (but the mean velocity is still null). Results for this case with $\beta = 0.05$ are shown in Fig. 10. As with the Riemann shock problem, 8-node quadrature does not predict the correct behavior for q_1. In contrast, with 27- and 64-node quadrature the results are very similar to each other, indicating that 27-node quadrature suffices for this value of β. For larger β, the presence of discontinuous initial velocity abscissas has ramifications on the realizability of the reconstructed distribution function. For example, with $\beta = \infty$ we find that some of the weights with 27- and 64-node quadrature become negative. Thus, in order to

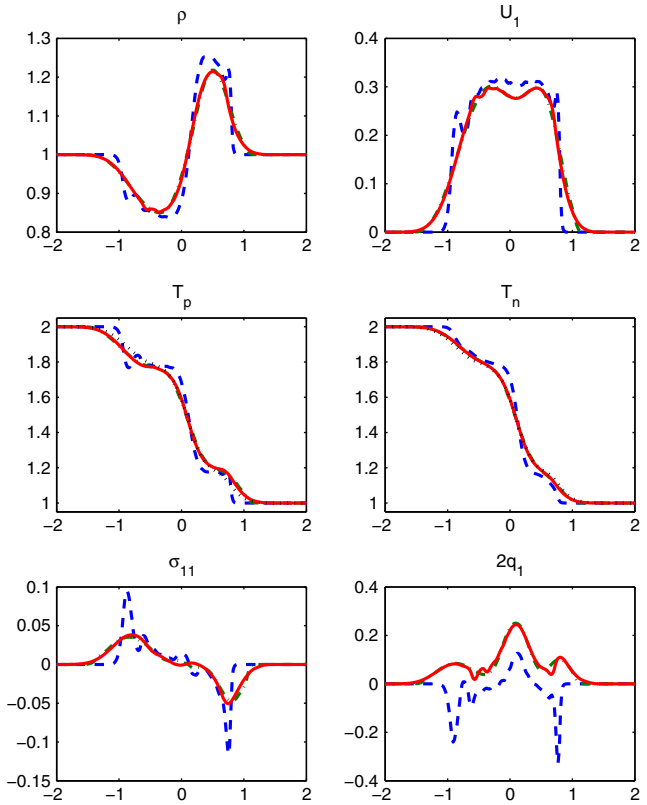

Fig. 10. Selected moments for the temperature shock problem at $t = 0.5$ with $\beta = 0.05$. Dashed line (blue): 8-node quadrature. Dash-dot line (green): 27-node quadrature. Solid line (red): 64-node quadrature. Dotted line (black): Particle temperature. (For interpretation of the references in colour in this figure legend, the reader is referred to the web version of this article.)

treat cases that are weakly collisional with 27- or 64-node quadrature, it will be necessary to devise an algorithm to treat negative weights as was done in [21] for 8-node quadrature.

6. Discussion and conclusions

In this work we have extended the 8-node quadrature method of moments for approximating solutions to the kinetic equation developed in [21] to higher-order velocity moments. The key technical challenge was the formulation of a moment-inversion algorithm for n^3 nodes where $n \in (1, 2, \ldots)$. In 3-D, the moment-inversion algorithm constructs three 1-D quadratures using the PD algorithm in each direction, and forms the 3-D velocity abscissas as a tensor product of the 1-D abscissas. The weights are then determined from a linear system using mixed moments with indices up to $n-1$. For a joint Gaussian distribution, the resulting quadrature coincides with the Gauss–Hermite quadrature. More generally, the three univariate quadratures are guaranteed to have non-negative weights and, hence, can be used to construct a realizable delta-function representation of the velocity distribution function. As shown in [29], the univariate quadratures offer optimal and bounded estimates of the higher-order moments, while exactly reproducing the lower-order moments. In 3-D, the maximum number of velocity moments that can be exactly controlled with the n^3-node tensor-product quadrature is $(n^2+3)n$, as compared to $4n^3$ for a non-tensor-product quadrature [22,23]. Despite this significant reduction in the number of moments that can be controlled for a given n, the moment-inversion algorithm based on a tensor product is very robust and computationally efficient, and thus well suited for use in a flow solver based on moment transport equations.

In order to investigate the properties of solutions to the kinetic equation found with the quadrature-based moment closure, we have used the Riemann shock problem with a linear (BGK) collision term. The resulting moment transport equation of order γ (Eq. (6)) is closed except for the moments of order $\gamma+1$ in the spatial fluxes, which are closed using quadrature. Thus, it is possible to examine directly how the number of nodes used in the quadrature method of moments affects the quality of the closure for the spatial fluxes. As shown in [21], the quadrature-based moment method can be used for arbitrary Mach and Knudsen numbers (i.e., the solutions remain realizable but not necessarily accurate). Of particular interest in this work was how the accuracy of the solutions depends on n for relatively large Mach and Knudsen numbers. As noted in the Introduction, the behavior of the quadrature-based moment method for low Mach and/or low Knudsen numbers will be identical to the off-lattice Boltzmann [1] and gas-kinetic methods [64], respectively.

The simulation results for the Riemann shock problem over a large range of Mach and Knudsen numbers have led to the following conclusions:

(1) The heat flux (q_1) predicted by the 8-node quadrature is incorrect. We attribute this problem to the fact that many of the third-order moments are not included in 8-node quadrature. Indeed, the heat fluxes for 27- and 64-node quadratures have the correct forms.
(2) For 8-node quadrature and sufficiently large Mach numbers the spatial fluxes are not well predicted, leading to discontinuities in the lower-order moments (e.g., density, mean velocity). Such problems are never observed with 27- and 64-node quadrature, even at very large Mach numbers.
(3) For relatively low Knudsen numbers, the predictions of the 27- and 64-node quadratures are in good agreement. However, as the Knudsen number is increased, the results for the two quadratures differ significantly. Presumably, because it controls more moments, the 64-node quadrature should be more accurate.
(4) At large (infinite) Knudsen number, the discrete nature of the quadrature-based closure for the spatial fluxes is clearly observed. As discussed in [23], for infinite Knudsen number (collision-less particles) each velocity abscissas obeys a separate pressure-less gas dynamics equation [5], which is known to produce delta shocks [6] and vacuum states [11]. Because of the strong dependence of solutions to the collision-less kinetic equation on initial and boundary conditions, it is unlikely that *any* moment method can provide an accurate solution for all cases. However, quadrature-based moment methods can provide an "optimal" solution for a finite set of moments. For example, highly non-equilibrium behavior such as jet crossing [16] can be accurately reproduced [13,39].
(5) For large Knudsen numbers (i.e., weakly collisional flows), we have observed negative weights in the moment-inversion algorithm. It will thus be necessary to treat such cases by setting the offending weights to zero removing one or more of the mixed moments from the linear system used to determine the weights. However, because the 1-D quadratures always yield non-negative weights, we are guaranteed that it will always be possible to find a reduced linear system with non-negative weights. Generally, in weakly collisional flows, the accuracy of the quadrature-based moment solution degrades (due to the discrete representation of the spatial fluxes) well before negative weights are observed.

We remind the reader that the Riemann shock problem does not require any special treatment to find the rotated central moments used in the moment-inversion algorithm. In general, however, it will be necessary either to solve for the rotated central moments directly or to compute them from the full set of central moments of order $\gamma = 3n-3$. (For more details, see [21] where the procedure for $n=2$ is described.)

In work to be reported elsewhere, we have shown that the quadrature-based moment method described here has (as expected) for low-Mach-number Poiseuille and Couette flows the same dependence on Knudsen number as higher-order

lattice Boltzmann methods [35]. We have also applied the algorithms described in this work to simulate granular flows far from equilibrium and found good agreement with discrete particle simulations [26,33]. Finally, we reiterate that the quadrature-based moment method presented in this work can be applied to any kinetic equation that is closed in terms of the velocity distribution function, including, for example, the full Boltzmann collision term [59], the Enskog-Boltzmann equation describing moderately dense granular gases [10,28], the Williams spray equation [15,23,62], and the kinetic equation for fluid-particle flows with finite Stokes number [16,21,54]. Thus, using the moment-inversion algorithm developed in this work, it will be possible to systematically investigate the number of velocity moments needed to accurately capture flows for any Knudsen, Mach and Stokes numbers. In conclusion, we note that the spatial accuracy of the numerical algorithm for the moment transport equations can be improved by using higher-order finite-volume schemes for the spatial fluxes [40,60], and for this we can make use of the previous work on higher-order methods for gas-kinetic schemes [47,48].

Acknowledgment

This work was supported by a Grant from the US National Science Foundation (CCF-0830214).

Appendix A. Product-difference algorithm

The product-difference (PD) algorithm was introduced by [29] as an efficient method to compute quadrature weights and abscissas for univariate distribution functions on finite intervals. The method relies on the theory of canonical moments [17], and the relationship between the canonical moments and the zeros of orthogonal polynomials [18,55]. Solving for the roots directly from the moments is ill-conditioned, so instead the PD algorithm solves an eigenvalue problem for a (symmetric, tridiagonal) Jacobi matrix constructed from the moments [52]. The abscissas are the eigenvalues and the weights are found from the first components of the eigenvectors [29]. As long at the (canonical) moments are realizable, the weights will be non-negative and the abscissas will lie in the interval on which the distribution is defined [17,55]. The PD algorithm described in [45] requires a separate treatment for cases where the first-order moment is null [61] (which covers all of the cases considered in this work). For completeness, we will thus provide explicit formulas for the Jacobi matrix up to $n = 4$.

Let the normalized central moments be denoted by $(1, 0, m_2, \ldots, m_7)$, and the elements of the Jacobi matrix by $z(i,j)$. Up to $n = 4$, the unique components of the Jacobi matrix are

$$\begin{aligned} &z(1,1) = q_1, \\ &z(2,2) = q_3/q_2,\ z(1,2) = \sqrt{q_2}, \\ &z(3,3) = q_5/q_4/q_2,\ z(2,3) = \sqrt{q_4}/q_2, \\ &z(4,4) = q_7/q_6/q_4,\ z(3,4) = \sqrt{q_2 q_6}/q_4, \end{aligned} \tag{A.1}$$

where the q_i are defined in terms of the moments:

$$\begin{aligned} q_1 &= 0, \\ q_2 &= m_2, \\ q_3 &= m_3, \\ q_4 &= -m_3^2 + (m_4 - m_2^2)m_2, \\ q_5 &= m_3^3 + (-2m_4m_3 + m_5m_2)m_2, \\ q_6 &= -m_4^3 + (2m_5m_4 + (-m_6 + m_3^2)m_3)m_3 + (m_4m_6 - m_5^2 - 3m_4m_3^2 + (2m_5m_3 + m_4^2 - m_6m_2)m_2)m_2, \\ q_7 &= (-m_4^4 + (3m_5m_4^2 + (-m_5^2 - 2m_6m_4 + m_7m_3)m_3)m_3)m_3 + (((-2m_5^2 + 2m_6m_4)m_4 + (2m_6m_5 - 2m_4m_7)m_3)m_3 \\ &\quad + (m_5^3 + (-2m_6m_5 + m_4m_7)m_4 \\ &\quad + (-2m_4^3 + (4m_5m_4 + (-2m_6 + m_3^2)m_3)m_3)m_3 + (2m_5m_4^2 + (-4m_5^2 + (2m_7 - 4m_4m_3)m_3)m_3 \\ &\quad + (2m_5m_6 - 2m_4m_7 + (3m_4^2 + 3m_5m_3)m_3 + (-2m_6m_3 - 2m_5m_4 + m_7m_2)m_2)m_2)m_2)m_2. \end{aligned} \tag{A.2}$$

Note that q_2, q_4 and q_6 will be non-negative for realizable moments, and will be zero only for degenerate distribution functions composed of delta functions. For example, $q_2 = 0$ can be represented by one delta function (i.e., zero variance). In most applications, these quantities will be positive.

For higher-order 1-D quadrature (i.e., $n > 4$), the Wheeler algorithm [61] described in [52] can be recommended. This algorithm requires the modified moments ν_j, and the recurrence coefficients α_j and β_j for a chosen basis of orthogonal polynomials π_j. A convenient choice is $\alpha_j = 0, \beta_j = 0$ and $\nu_j = m_j$. The subroutine `orthog` in [52] takes as input

$$\nu_i \text{ for } i \in (0, 1, \ldots, 2n-1) \quad \text{and} \quad \alpha_i, \beta_i \text{ for } i \in (0, 1, \ldots, n-1),$$

and uses the Wheeler algorithm to compute the recurrence coefficients a_i, b_i for $i \in (0, 1, \ldots, n-1)$. Note that for realizable moments, $b_i \geqslant 0$. The recurrence coefficients are then used to define the Jacobi matrix:

$$z(i,i) = a_{i-1} \text{ for } i \in (1,2,\ldots,n),$$
$$z(i,i+1) = \sqrt{b_i} \text{ for } i \in (1,2,\ldots,n-1), \tag{A.3}$$
$$z(i+1,i) = \sqrt{b_i} \text{ for } i \in (1,2,\ldots,n-1).$$

The n eigenvalues of the Jacobi matrix are the desired abscissas, and the first component of the corresponding eigenvector w_j yields the weight: $\rho_j = m_0 w_j^2$. The algorithm `gaucof` in [52] can be used for this purpose. Note that by definition the eigenvalues are real and the weights are non-negative. As discussed in [61], the Wheeler algorithm computes a_j and b_j to machine accuracy for large n, thereby avoiding the ill-conditioning associated with a direct moment-inversion method. Note that the Wheeler algorithm with standardized Gaussian moments will generate weights and abscissas equal to the Gauss–Hermite quadrature. We have used this fact to verify our numerical implementation.

References

[1] A. Bardow, I.V. Karlin, A.A. Guzev, Multispeed models in off-lattice Boltzmann simulations, Physical Review E 77 (2008) 025701 (R).
[2] A.E. Beylich, Solving the kinetic equation for all Knudsen numbers, Physics of Fluids 12 (2000) 444–465.
[3] P.L. Bhatnagar, E.P. Gross, M. Krook, A model for collision processes in gases. I. Small amplitude processes in charged and neutral one-component systems, Physical Reviews 94 (1954) 511–525.
[4] G.A. Bird, Molecular Gas Dynamics and the Direct Simulation of Gas Flows, Clarendon, Oxford, 1994.
[5] F. Bouchut, On zero pressure gas dynamics, Advances in Kinetic Theory and Computing. Series on Advances in Mathematics for Applied Sciences 22 (1994) 171–190.
[6] F. Bouchut, S. Jin, X.T. Li, Numerical approximations of pressureless gas and isothermal gas dynamics, SIAM Journal of Numerical Analysis 41 (2003) 135–158.
[7] J.E. Broadwell, Shock structure in a simple discrete velocity gas, The Physics of Fluids 7 (8) (1964) 1243–1247.
[8] C. Cercignani, The Boltzmann Equation and its Applications, Springer, New York, 1988.
[9] C. Cercignani, Rarefied Gas Dynamics, Cambridge University Press, Cambridge, 2000.
[10] S. Chapman, T.G. Cowling, The Mathematical Theory of Nonuniform Gases, Cambridge University Press, Cambridge, 1970.
[11] G.-Q. Chen, H. Liu, Formation of δ-shocks and vacuum states in the vanishing pressure limit of solutions to the Euler equations for isentropic fluids, SIAM Journal of Mathematical Analysis 34 (2003) 925–938.
[12] C.K. Chu, Kinetic-theoretic description of the formation of a shock wave, The Physics of Fluids 8 (1965) 12–22.
[13] S. de Chaisemartin, L. Fréret, D. Kah, F. Laurent, R.O. Fox, J. Reveillon, M. Massot, Turbulent combustion of polydisperse evaporating sprays with droplet crossing: Eulerian modeling and validation in the infinite Knudsen limit, in: Proceedings of the Summer Program 2008, Center for Turbulence Research, Stanford, 2008, pp. 265–276.
[14] S. Deshpande, A second order accurate, kinetic theory based, method for inviscid compressible flows. Technical Report NASA Langley 2613, 1986.
[15] O. Desjardins, R.O. Fox, P. Villedieu, A quadrature-based moment closure for the Williams spray equation, in: Proceedings of the Summer Program 2006, Center for Turbulence Research, Stanford, 2006, pp. 223–234.
[16] O. Desjardins, R.O. Fox, P. Villedieu, A quadrature-based moment method for dilute fluid-particle flows, Journal of Computational Physics 227 (2008) 2514–2539.
[17] H. Dette, W.J. Studden, The Theory of Canonical Moments with Applications in Statistics, Probability, and Analysis, Wiley, New York, 1997.
[18] J. Favard, Sur les polynomes de Tchebicheff, Comptes Rendus de l'Académie des Sciences, Paris 200 (1935) 2052–2053.
[19] R.O. Fox, Computational Models for Turbulent Reacting Flows, Cambridge University Press, Cambridge, 2003.
[20] R.O. Fox, Bivariate direct quadrature method of moments for coagulation and sintering of particle populations, Journal of Aerosol Science 37 (2006) 1562–1580.
[21] R.O. Fox, A quadrature-based third-order moment method for dilute gas-particle flows, Journal of Computational Physics 227 (2008) 6313–6350.
[22] R.O. Fox, Optimal moment sets for multivariate quadrature-based moment methods, Industrial & Engineering Chemistry Research (2009), doi:10.1021/ie801316d.
[23] R.O. Fox, F. Laurent, M. Massot, Numerical simulation of spray coalescence in an Eulerian framework: direct quadrature method of moments and multi-fluid method, Journal of Computational Physics 227 (2008) 3058–3088.
[24] L. Fréret, F. Laurent, S. de Chaisemartin, D. Kah, R.O. Fox, P. Vedula, J. Reveillon, O. Thomine, M. Massot, Turbulent combustion of polydisperse evaporating sprays with droplet crossing: Eulerian modeling of collisions at finite Knudsen and validation, in: Proceedings of the Summer Program 2008. Center for Turbulence Research, Stanford, 2008, pp. 277–288.
[25] U. Frisch, D. d'Humières, B. Hasslacher, P. Lallemand, Y. Pomeau, J.-P. River, Lattice gas hydrodynamics in two and three dimensions, Complex Systems 1 (4) (1987) 649–707.
[26] J.E. Galvin, C.M. Hrenya, R.D. Wildman, On the role of the Knudsen layer in rapid granular flows, Journal of Fluid Mechanics 585 (2007) 73–92.
[27] R. Gatignol, Théorie cinétique d'un gaz à répartition discrète de vitesses. Lecture Notes in Physics 36, Springer, Berlin, 1975.
[28] I. Goldhirsch, Rapid granular flows, Annual Review of Fluid Mechanics 35 (2003) 267–293.
[29] R.G. Gordon, Error bounds in equilibrium statistical mechanics, Journal of Mathematical Physics 9 (1968) 655–662.
[30] H. Grad, On the kinetic theory of rarefied gases, Communications on Pure and Applied Mathematics 2 (1949) 331–407.
[31] Z. Guo, H. Liu, L.-S. Luo, K. Xu, A comparative study of the LBE and GKS methods for 2D near incompressible laminar flows, Journal of Computational Physics 227 (2008) 4955–4976.
[32] N.G. Hadjiconstantinou, The limits of Navier-Stokes theory and kinetic extensions for describing small-scale gaseous hydrodynamics, Physics of Fluids 18 (2006) 111301.
[33] C.M. Hrenya, J.E. Galvin, R.D. Wildman, Evidence of higher-order effects in thermally driven rapid granular flows, Journal of Fluid Mechanics 598 (2008) 429–450.
[34] J.T. Jenkins, S.B. Savage, A theory for the rapid flow of identical, smooth, nearly elastic spherical particles, Journal of Fluid Mechanics 130 (1983) 187–202.
[35] S.H. Kim, H. Pitsch, I.D. Boyd, Accuracy of higher-order lattice Boltzmann methods for microscale flows with finite Kundsen numbers, Journal of Computational Physics 227 (2008) 8655–8671.
[36] P. Lallemand, L.-S. Luo, Theory of the lattice Boltzmann method: dispersion, dissipation, isotropy, Galilean invariance, and stability, Physical Review E 68 (3) (2003) 036706.
[37] F. Laurent, M. Massot, Multi-fluid modeling of laminar poly-dispersed spray flames: origin, assumptions and comparison of the sectional and sampling methods, Combustion Theory and Modelling 5 (2001) 537–572.
[38] F. Laurent, M. Massot, P. Villedieu, Eulerian multi-fluid modeling for the numerical simulation of coalescence in polydisperse dense liquid sprays, Journal of Computational Physics. 194 (2004) 505–543.
[39] N. Le Lostec, R.O. Fox, O. Simomin, P. Villedieu, Numerical description of dilute particle-laden flows by a quadrature-based moment method, in: Proceedings of the Summer Program 2008. Center for Turbulence Research, Stanford, 2008, pp. 209–221.

[40] R. Leveque, Finite Volume Methods for Hyperbolic Problems, Cambridge University Press, Cambridge, 2002.
[41] C.D. Levermore, Moment closure hierarchies for kinetic theories, Journal of Statistical Physics 83 (1996) 1021–1065.
[42] D.L. Marchisio, R.O. Fox, Solution of population balance equations using the direct quadrature method of moments, Journal of Aerosol Science 36 (2005) 43–73.
[43] D.L. Marchisio, J.T. Pikturna, R.O. Fox, R.D. Vigil, A.A. Barresi, Quadrature method of moments for population balances with nucleation, growth and aggregation, AIChE Journal 49 (2003) 1266–1276.
[44] D.L. Marchisio, R.D. Vigil, R.O. Fox, Quadrature method of moments for aggregation-breakage processes, Journal of Colloid and Interface Science 258 (2) (2003) 322–334.
[45] R. McGraw, Description of aerosol dynamics by the quadrature method of moments, Aerosol Science and Technology 27 (1997) 255–265.
[46] R. McGraw, Numerical advection of correlated tracers: preserving particle size/composition moment sequences during transport of aerosol mixtures. Journal of Physics: Conference Series 78 (2007) 012045.
[47] G. Ni, S. Jiang, K. Xu, Efficient kinetic schemes for steady and unsteady flow simulations on unstructured meshes, Journal of Computational Physics 227 (2008) 3013–3031.
[48] G. Ni, S. Jiang, K. Xu, A DGBGK scheme based on WENO limiters for viscous and inviscid flows, Journal of Computational Physics 227 (2008) 5799–5815.
[49] I. Nicodin, R. Gatignol, Unsteady half-space evaporation and condensation problems on the basis of the discrete kinetic theory, Physics of Fluids 18 (2006) 127105.
[50] Y. Ogata, H.-N. Im, T. Yabe, Numerical method for Boltzmann equation with Soroban-grid CIP method, Communications in Computational Physics 2 (4) (2007) 760–782.
[51] B. Perthame, Boltzmann type schemes for compressible Euler equations in one and two space dimensions, SIAM Journal of Numerical Analysis 29 (1) (1990) 1–19.
[52] W.H. Press, S.A. Teukolsky, W.T. Vetterling, B.P. Flannery, Numerical Recipes in Fortran 77: The Art of Scientific Computing, Cambridge University Press, Cambridge, 1992.
[53] D.I. Pullin, Direct simulation methods for compressible inviscid ideal gas-flows, Journal of Computational Physics 34 (1980) 53–66.
[54] M. Sakiz, O. Simonin, Numerical experiments and modelling of non-equilibrium effects in dilute granular flows, in: Proceedings of the 21st International Symposium on Rarefied Gas Dynamics, Cépaduès-Éditions, Toulouse, France, 1998.
[55] J.A. Shohat, J.D. Tamarkin, The problem of moments. Mathematical Surveys 1, American Mathematical Society, Providence, 1943.
[56] A.H. Stroud, Approximate Calculation of Multiple Integrals, Prentice-Hall, Englewood Cliffs, 1971.
[57] H. Struchtrup, Macroscopic Transport Equations for Rarefied Gas Flows, Springer, New York, 2005.
[58] M. Torrilhon, H. Struchtrup, Regularized 13-moment equations: shock structure calculations and comparison to Burnett models, Journal of Fluid Mechanics 513 (2004) 171–198.
[59] P. Vedula, R.O. Fox, I.D. Boyd, A quadrature-based method of moments for solution Boltzmann equation, submitted for publication.
[60] V. Vikas, Z.J. Wang, R.O. Fox, A. Passalacqua, High-order realizable finite-volume schemes for quadrature-based moment method, in: 48th AIAA Aerospace Sciences Meeting, submittedfor publication.
[61] J.C. Wheeler, Modified moments and Gaussian quadratures, Rocky Mountain Journal of Mathematics 4 (1974) 287–296.
[62] F.A. Williams, Spray combustion and atomization, Physics of Fluids 1 (1958) 541–545.
[63] D.L. Wright, Numerical advection of moments of the particle size distribution in Eulerian models, Journal of Aerosol Science 38 (2007) 352–369.
[64] K. Xu, A gas-kinetic BGK scheme for the Navier-Stokes equations and its connection with artificial dissipation and Godunov method, Journal of Computational Physics 171 (2001) 289–335.
[65] K. Xu, X. He, C. Cai, Multiple temperature kinetic model and gas-kinetic method for hypersonic non-equilibrium flow computations, Journal of Computational Physics 227 (2008) 6779–6794.
[66] C. Yoon, R. McGraw, Representation of generally mixed multivariate aerosols by the quadrature method of moments: I, Statistical foundation. Journal of Aerosol Science 35 (2004) 561–576.